

1 **Do Land Models Miss Key Soil Hydrological Processes Controlling Soil Moisture Memory?**

2  
3 **Mohammad A. Farmani<sup>1</sup>, Ali Behrangi<sup>1,2</sup>, Aniket Gupta<sup>1</sup>, Ahmad Tavakoly<sup>3,4</sup>, Matthew**  
4 **Geheran<sup>3</sup>, and Guo-Yue Niu<sup>1</sup>**

5  
6  
7 <sup>1</sup>Department of Hydrology and Atmospheric Sciences, University of Arizona, Tucson, AZ, USA,

8 <sup>2</sup>Department of Geosciences, University of Arizona, Tucson, AZ, USA,

9 <sup>3</sup>US Army Engineer Research and Development Center, Coastal and Hydraulics Laboratory,  
10 Vicksburg, MS, USA,

11 <sup>4</sup>Earth System Science Interdisciplinary Center, University of Maryland, College Park, MD,  
12 USA

13  
14  
15  
16  
17 Corresponding author: Mohammad Farmani, email: [farmani@arizona.edu](mailto:farmani@arizona.edu)

18 Guo-Yue Niu, email: [niug@arizona.edu](mailto:niug@arizona.edu)

19  
20  
21  
22  
23  
24  
25  
26  
27  
28  
29  
30  
31  
32  
33  
34  
35  
36  
37  
38  
39 **Key Points:**

40 Van-Genuchten soil hydraulics improves long-term Soil Moisture Memory (SMM) of the  
41 topsoil.

42 Explicitly representing surface ponding and its infiltration enhances soil moisture memory in  
43 both topsoil and the root zone.

44 Representing preferential flow improves both short-term and long-term SMM in both the  
45 topsoil and root zone.

46       **Abstract**

47  
48       Soil moisture memory (SMM), which refers to how long a perturbation in Soil Moisture (SM) can  
49       last, is critical for understanding climatic, hydrologic, and ecosystem interactions. Most land  
50       surface models (LSMs) tend to overestimate surface soil moisture and its persistency (or SMM),  
51       sustaining spuriously large soil surface evaporation during dry-down periods. We attempt to  
52       answer a question: Do LSMs miss or misrepresent key hydrological processes controlling SMM?  
53       We use a version of Noah-MP with advanced hydrology that explicitly represents preferential flow  
54       and surface ponding and provides optional schemes of soil hydraulics. We test the effects of these  
55       processes that are generally missed by most LSMs on SMM. We compare SMMs computed from  
56       various Noah-MP configurations against that derived from the Soil Moisture Active Passive  
57       (SMAP) Level 3 soil moisture and in-situ measurements from the International Soil Moisture  
58       Network (ISMN) from year 2015 to 2019 over the contiguous United States (CONUS). The results  
59       suggest that 1) soil hydraulics plays a dominant role, and the Van-Genuchten hydraulic scheme  
60       reduces the overestimation of the long-term surface SMM produced by the Brooks-Corey scheme,  
61       which is commonly used in LSMs; 2) explicitly representing surface ponding enhances SMM for  
62       both the surface layer and the root zone; and 3) representing preferential flow improves the overall  
63       representation of soil moisture dynamics. The combination of these missing schemes can  
64       significantly improve the long-term memory overestimation and short-term memory  
65       underestimation issues in LSMs. We suggest that LSMs for use in seasonal-to-subseasonal climate  
66       prediction should, at least, adopt the Van-Genuchten hydraulic scheme.

67  
68  
69  
70  
71  
72  
73  
74  
75  
76  
77  
78  
79  
80  
81  
82  
83  
84  
85  
86  
87  
88  
89  
90  
91  
92  
93  
94

95 **Plain Language Summary**

96

97 Land surface models (LSMs) represent the physical and bio-geochemical exchanges of mass and  
98 energy between surface and atmosphere. Such exchanges are extensively dependent on the surface  
99 soil water amount and its persistence. This study explores key hydrological processes that may be  
100 missed by LSMs but important for weather and climate predictions. Through virtual experiments  
101 with a state-of-the-art model, we found that soil hydraulics (representing how efficiently soil can  
102 hold/release water under varying pressure) is particularly effective in sustaining soil moisture.  
103 Additionally, we found that allowing water to pond on the soil surface helps improve the model's  
104 soil moisture persistency. Furthermore, enhanced soil permeability due to soil macropores also  
105 regulates the water movement hence improving the soil moisture persistency. Overall, future  
106 LSMs should refine the treatment of soil water retention capability and consider the effects of soil  
107 macropores and surface ponding to improve weather and seasonal climate predictions.

108

## 109 1. Introduction

110

111 Land surface models' (LSMs) efficacy in simulating climate feedback mechanisms critically  
112 depends on the soil water retention capacity and soil moisture persistency. The influence of soil  
113 moisture on climate predictions at seasonal-to-sub-seasonal (S2S) scales is well-recognized due to  
114 its role in the exchange of surface energy and water fluxes with the atmosphere (Koster and Suarez  
115 2001, Koster, Dirmeyer et al. 2002, Koster, Guo et al. 2009, Koster, Mahanama et al. 2010). Water  
116 stored in soil and aquifers, which variably persists from seasons to years, is known to affect  
117 precipitation variability (Koster and Suarez 1999, Koster and Suarez 2001). This impact is  
118 particularly pronounced in regions transitioning from dry to wet conditions, where  
119 evapotranspiration (ET) is highly sensitive to soil moisture levels (Koster and Suarez 2001, Koster,  
120 Dirmeyer et al. 2004, Guo, Dirmeyer et al. 2006, Seneviratne, Koster et al. 2006). While the nature  
121 and scale of soil moisture-precipitation feedback are still being debated (Findell, Gentine et al.  
122 2011, Taylor, Birch et al. 2013), numerous studies have emphasized the importance of soil  
123 moisture initialization and its persistency for accurate climate predictions (Zeng, Liu et al. 2010,  
124 Dirmeyer 2011, Mei and Wang 2012, Shellito, Small et al. 2016, Tuttle and Salvucci 2016, Yousefi  
125 Sohi, Zahraie et al. 2024, Zebarjadian, Dolatabadi et al. 2024). The strength of soil moisture-  
126 precipitation coupling widely varies across different climate models (Koster and Suarez 1999,  
127 Koster, Dirmeyer et al. 2004, Seneviratne and Koster 2012, Taylor, Birch et al. 2013, Moghisi,  
128 Yazdi et al. 2024), and discrepancies in the modeled soil moisture by LSMs for climate modeling  
129 are notable (Boone 2004, Souri, OmidvarMohammadi et al. 2024).

130

131 Refinement of soil moisture-precipitation feedback in LSMs is hindered by the lack of large-scale  
132 observational data, challenging the improvement and validation of model simulations (Koster and  
133 Suarez 1999, Koster and Suarez 2001, Koster, Mahanama et al. 2010, Koster and P. Mahanama  
134 2012, Seneviratne and Koster 2012). This shortfall highlights the necessity for more detailed  
135 representations of land-atmosphere feedback mechanisms that are crucial for extreme weather  
136 event predictions, yet are typically parameterized rather than explicitly resolved in models  
137 (McColl, He et al. 2019, Pastorello, Trotta et al. 2020). Integrating extensive observational data is  
138 vital for simulating the intricacies of climate and weather and improving model predictive skill  
139 (Koster, Schubert et al. 2009, Koster, Reichle et al. 2017, Shellito, Small et al. 2018, McColl, He  
140 et al. 2019, Mohammadi, Zandi et al. 2023). Recent advancements in remote sensing observations  
141 have enabled analyses of interactions between near-surface soil and the atmosphere. Nonetheless,  
142 the paucity of root zone data complicates the investigation of deep soil dynamics. Numerous  
143 studies have utilized satellite soil moisture products to evaluate and refine models, focusing on the  
144 spatial and temporal patterns of soil moisture variability (Koster, Guo et al. 2009, Yang, Chen et  
145 al. 2020). In particular, the Soil Moisture Active Passive (SMAP) mission has been extensively  
146 employed to assess model performance (Shellito, Small et al. 2016, McColl, Alemohammad et al.  
147 2017, McColl, Wang et al. 2017, Shellito, Small et al. 2018, McColl, He et al. 2019).

148

149 The concept of Soil Moisture Memory (SMM)—the duration required for a perturbation, such as  
150 rainfall, to dissipate—becomes essential for understanding the land-atmosphere interactions.  
151 SMM encapsulates the temporal variations of soil moisture, reflecting the exchange of fluxes  
152 between land and atmosphere. Therefore, SMM is an important metric for evaluating LSMs, since  
153 one of their functions is to provide surface flux exchanges and boundary conditions for  
154 atmospheric models (Koster, Dirmeyer et al. 2004, Guo, Dirmeyer et al. 2006, Seneviratne, Koster

155 et al. 2006, Koster, Guo et al. 2009, Koster, Schubert et al. 2009). SMM also facilitates the  
156 comparison of how quickly soil loses water between observations and various models, providing  
157 insights into the mechanisms within LSMs and their hydrometeorological responses. Moreover,  
158 analyzing SMM can yield valuable data on the configurations and hydrological parameterizations  
159 of specific LSMs, thus improving our understanding of how different configurations impact model  
160 performance, particularly in soil moisture representation. For instance, Shellito et al. (2018)  
161 measured the drying rate of surface soil moisture, which they considered as soil moisture memory,  
162 using SMAP data and the Noah LSM during the initial 1.8 years following SMAP's launch. They  
163 concluded that Noah shows a slower drying rate and a longer surface SMM compared with SMAP,  
164 due likely to the too strong soil water suction represented by Noah.

165  
166 Determining SMM is not straightforward due to the variety of calculation methods proposed by  
167 researchers (Koster and Suarez 1999, Koster and Suarez 2001, Koster, Dirmeyer et al. 2002,  
168 Koster, Dirmeyer et al. 2004, Seneviratne, Koster et al. 2006, Katul, Porporato et al. 2007, Koster,  
169 Guo et al. 2009, Ghannam, Nakai et al. 2016, Shellito, Small et al. 2016, McColl, Alemohammad  
170 et al. 2017, McColl, Wang et al. 2017, McColl, He et al. 2019, Mao, Crow et al. 2020), each  
171 introducing its own level of uncertainty. Traditionally, soil moisture has been conceptualized as a  
172 red noise process, forming the basis for SMM calculations (T. L. Delworth & Manabe, 1988). This  
173 approach has led to the definition of SMM as the e-folding autocorrelation timescale within such  
174 a process (Delworth and Manabe 1989). SMM has also been characterized using various other  
175 autocorrelation-based methods, such as the integral timescale (Nakai, Katul et al. 2014, Ghannam,  
176 Nakai et al. 2016), soil moisture variance spectrum (Katul et al., 2007; Nakai et al., 2014), and the  
177 constant time lag autocorrelation (Koster and Suarez 2001, Seneviratne, Lüthi et al. 2006).  
178 Traditionally, these models were applied to monthly datasets. However, this approach risks  
179 overlooking dynamic processes governed by limitations in water and energy (Mccoll et al., 2019).  
180 Consequently, there has been a shift away from their use towards recent high-resolution  
181 observational and modeling data. Therefore, there is a need for further research to refine SMM  
182 measurement that can then be used as a benchmark for assessing LSMs (Mccoll et al., 2019).

183  
184 McColl et al. (2019) categorized soil water loss into two main categories: water-limited (long-  
185 term) and energy-limited (short-term). The energy-limited regime is a process where water loss is  
186 constrained by available energy and lasts from hours to a few days. In contrast, the water-limited  
187 regime is a process where water loss depends on the available water and spans longer periods, such  
188 as weeks, months, and seasons. McColl et al. (2019) specified that ET and drainage are the main  
189 controllers of long-term and short-term memories, respectively. Utilizing a two-year dataset from  
190 the SMAP mission and simulations from the Goddard Earth Observing System Model, Version 5  
191 (GEOS-5), McColl et al. (2019) conducted a global analysis under various climatic and land  
192 conditions. Their analysis revealed that GEOS-5 tends to overpredict the duration of water-limited  
193 memory and underpredicts energy-limited memory compared to SMM inferred from SMAP data,  
194 while the results were not affected by the SMAP sampling frequency of 3 days. Building on this,  
195 He et al. (2023) employed the hybrid memory approach proposed by McColl et al. (2019) to assess  
196 the hydrometeorological response of various LSMs, including GLDAS-CLSM, GLDAS-Noah,  
197 MERRA2, NCEP, ERA5, and JRA55, against SMAP observations for 2015 – 2020. The authors  
198 observed that LSMs generally overestimate memory in water-limited regime and significantly  
199 underestimate it in energy-limited regime. Moreover, their study suggested that discrepancies in  
200 SMM representation within LSMs are more attributable to the physical processes incorporated

201 rather than factors such as soil layer thickness or the nature of model simulations (online/offline)  
202 (He, Lu et al. 2023).

203

204 A recent review on SMM identified the soil properties and processes as an important controlling  
205 factor of SMM in addition to atmospheric forcings, land use and management for future studies to  
206 examine the fundamental mechanisms of SMM emergence (Rahmati et al., 2024). Based on the  
207 works of McColl et al. (2019) and He et al. (2023), this study aims to examine the impacts of key  
208 soil hydrological processes and soil hydraulics on SMM that may be missed in most LSMs. Current  
209 LSMs may be not enough to address the uncertainties of SMM estimates for incomplete  
210 representations of key hydrological processes controlling SMM and uncertainties in soil hydraulic  
211 parameters (Rahmati et al., 2024). As such, we use a version of Noah-MP with advanced  
212 hydrological representations of preferential flow, surface ponding, runoff of surface ponded water  
213 (infiltration excess runoff), and lateral infiltration, etc. (Niu et al., 2024). We conduct model  
214 experiments with various soil hydraulic parametrizations of those by Brooks and Corey (1964) and  
215 Van-Genuchten (1980), preferential flow, and surface ponding depth. Our analysis investigates the  
216 impact of these configurations on soil moisture persistency across ET regimes and drainage, so  
217 that it can provide insight into these missing physical processes affecting SMM. By comparing  
218 SMM produced by various settings of Noah-MP with SMAP Level 3 data and ISMN observations  
219 from 2015 to 2019 over the CONUS, we seek to identify key processes and soil hydraulic schemes  
220 controlling SMM and thus provide guidance for future developments of LSMs (e.g., reduce the  
221 prevalent SMM overestimations in LSMs).

222

## 223 **2. Materials and Methods**

224

225 SMM denotes the duration required for a perturbation to dissipate, or the period from the start to  
226 the end of a perturbation. For instance, following precipitation, the change in near-surface soil  
227 moisture marks the beginning of the perturbation. This excess moisture gradually diminishes due  
228 to flux exchange or percolation to deeper soil layers. The moisture level of soil plays a critical  
229 role in influencing water loss patterns. Following rainfall, the upper layer of soil initially holds  
230 more moisture than its field capacity ( $\theta_{fc}$ ), causing runoff and drainage (see Figure 1a).  
231 Subsequently, as the soil gradually dries, its moisture content reduces to a range between  $\theta_{fc}$  and  
232 the critical threshold ( $\theta_c$ ). This phase leads to consistent water loss at the maximum ET rate, known  
233 as Stage-I ET. As this process continues, the soil moisture falls below  $\theta_c$  (Figure 1a), at which  
234 stage ET becomes limited by the available water, termed Stage-II ET or ET at water-limited regime  
235 (illustrated in Figure 1a & b). Ultimately, when the soil moisture drops below the wilting point  
236 ( $\theta_w$ ), water no longer leaves the soil. Therefore, the whole process of water loss depends on the  
237 soil's moisture level and falls into two main types: energy-limited including unresolved drainage,  
238 and Stage-I ET, and water-limited including Stage-II ET (Figure 1b) (Mccoll et al., 2019; He et al.  
239 2023). Energy-limited, green strips, and water-limited regimes, dotted-lines, are shown in soil  
240 moisture times series at the Tonzi Ranch station (Figure 1c).

241

242

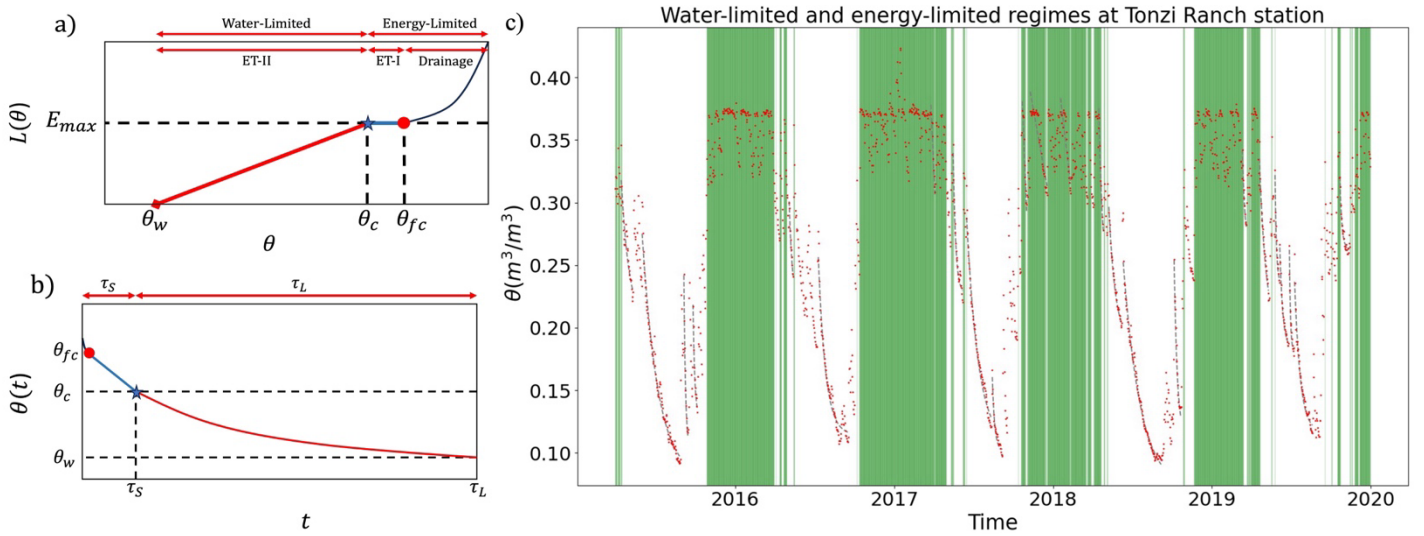


Figure 1 Schematic diagrams of (a) surface water loss process and (b) soil moisture memory at different soil moisture regimes [adapted from (McColl, Wang, et al., 2017b)]. Note that the x-axis in (a) refers to soil moisture ( $\text{m}^3\text{m}^{-3}$ ), and y-axis refers to surface water loss rate,  $L(\theta)$  (mm/s);  $E_{\max}$  is the maximum evaporation rate (mm/s). In (b), x-axis refers to time (e.g., days) and y-axis to SM content ( $\text{m}^3\text{m}^{-3}$ ). Panel (c) shows the SM time series for the Tonzi Ranch station, with green periods indicating energy-limited regime and dotted lines representing water-limited regime.  $\theta_w$ ,  $\theta_c$  and  $\theta_{fc}$  refer to the wilting point, critical point, and field capacity, respectively.

243  
244

## 245 2.1. Soil Moisture Memory of Water-Limited Regime ( $\tau_L$ ) and Energy-Limited 246 Regime ( $\tau_S$ )

247

248 McColl et al. (2019) considered the SMM concept as it relates to two regimes: a) the memory of  
249 water-limited regime ( $\tau_L$ ), specified by 'L' abbreviation of Long-term, b) the memory of energy-  
250 limited regime ( $\tau_S$ ), specified by 'S' abbreviation of Short-term. Their model incorporates a  
251 deterministic equation to represent water-limited processes during soil moisture drydown periods.  
252 However, energy-limited processes occur over shorter timescales and present a challenge for  
253 current satellite technologies to provide precise observations. McColl et al. (2019) highlighted that  
254 drainage is not a completely resolved process by satellite observations. To address this gap,  
255 McColl et al. (2019) proposed a stochastic equation to capture the unresolved nature of energy-  
256 limited processes.

257

258 The hybrid model is formulated by McColl et al. (2019) as follows:

$$\frac{d\theta(t)}{dt} = \begin{cases} \frac{-\theta(t) - \theta_w}{\tau_L}, P = 0 \\ \frac{-\theta(t) - \bar{\theta}}{\tau_S} + \varepsilon(t), P > 0 \end{cases} \quad (1)$$

259 where,  $\theta$  is the volumetric soil moisture,  $P$  indicates precipitation,  $\theta_w$  is the minimum soil moisture,  
 260  $\bar{\theta}$  is the time-averaged SM, and  $\varepsilon(t)$  is a random variable with a mean of zero.  $\tau_L$  and  $\tau_S$  are SMM  
 261 for the water-limited and energy-limited regimes, respectively. McColl et al. (2019) solved these  
 262 equations, demonstrating that the memories can be expressed as:

$$\theta(t) = \Delta\theta \exp\left(\frac{-t}{\tau_L}\right) + \theta_w P = 0 \quad (2)$$

$$\tau_S = \frac{-\frac{\Delta t}{2}}{\log} \quad (3)$$

263  $\Delta\theta$  represents the soil moisture changes during drydown,  $\Delta t$  is the temporal resolution of the soil  
 264 moisture data,  $\alpha$  is the precipitation intensity,  $\Delta z$  is soil layer thickness, and  $\overline{\Delta\theta_+} = \theta(t) - \theta(t - \Delta t)$   
 265 represents a positive increment in soil moisture. (McColl, Alemohammad et al. 2017) defined  
 266  $\frac{\Delta z [\overline{\Delta\theta_+}]}{\alpha}$  as stored fraction of precipitation, indicating the average proportion of water that still exists  
 267 in soil layer  $\Delta t$  days after rainfall. McColl et al. (2019) declared that the short-term memory in  
 268 their hybrid model is dominated by drainage when the sampling is relatively high (as in the case  
 269 of SMAP's sampling frequency of 3 days). This approach and its rationale are further elaborated  
 270 in (McColl, Alemohammad et al. 2017) and McColl et al. (2019).  
 271

272  
 273 In the analysis of water-limited memory, we fitted Equation 2 to the soil moisture time series  
 274 during specific drydown intervals. Then,  $\tau_L$  was extracted as a parameter from the fitting curve  
 275 (black dotted lines in Figure 1c). In contrast, short-term memory was determined directly using  
 276 Equation 3, as indicated by the green periods in Figure 1c. Further information about the criteria  
 277 for calculating memories can be found in McColl et al. (2019).  
 278

## 279 **2.2. Description of Datasets**

280  
 281 We use high-resolution atmospheric forcing datasets to drive the Noah-MP LSM. This model is  
 282 set up to simulate soil moisture dynamics, featuring advanced infiltration and water retention  
 283 processes. Additionally, it includes a precise parameterization for ponding depth. This setup  
 284 facilitated five distinct experiments. Then, we used surface and root zone soil moisture data derived  
 285 from the Noah-MP experiments, SMAP Level 3 surface soil moisture measurements, and root zone  
 286 soil moisture measurements from the International Soil Moisture Network (ISMN) to calculate the  
 287 hybrid SMM. The rest of this section describes in detail the forcing and observational datasets, the  
 288 Noah-MP LSM configurations, the employed infiltration and water retention schemes, and the  
 289 ponding depth threshold criterion.  
 290  
 291

### 292 **2.2.1 Atmospheric Forcing, Soil and Vegetation Parameters**

293



294 For modeling purposes, this study utilized the North American Data Assimilation System Phase 2  
295 (NLDAS-2) near-surface meteorological data at an hourly interval and 0.125° spatial resolution.  
296 This dataset encompasses a range of variables including air temperature, specific humidity, wind  
297 speed, surface pressure, shortwave and longwave radiation, and precipitation (Xia, Mitchell et al.  
298 2012). We also used precipitation data from the Integrated Multi-satellite Retrievals for Global  
299 Precipitation Measurement (IMERG-Final) dataset (Huffman, Bolvin et al. 2020, Jawad,  
300 Bhattacharya et al. 2024, Yousefi Sohi, Farmani et al. 2024), which offers half-hourly  
301 measurements across a 0.1° grid extending from 60°S to 60°N. Subsequently, the IMERG-Final  
302 data were mapped to the 0.125° resolution of NLDAS-2 using bilinear interpolation. These  
303 precipitation data sources were integrated into the short-term SMM computation process. To  
304 integrate the IMERG precipitation product into the model, we modified the forcing component of  
305 the Noah-MP code. Specifically, an average of NLDAS-2 and IMERG precipitation was employed  
306 when NLDAS-2 reported negative precipitation values, which was particularly significant in  
307 coastal regions. This adjustment enhanced the accuracy of precipitation inputs, contributing to  
308 more reliable simulations in these areas.

309 To ascertain soil and vegetation parameters, the hybrid State Soil Geographic Database  
310 (STATSGO) with a 1-km resolution and the United States Geological Survey's (USGS) 24-  
311 category vegetation classification were employed. The datasets were aggregated to align with a  
312 0.125° resolution, which is consistent with the NLDAS-2 forcing data. This process included  
313 determining the dominant soil and vegetation types for each grid cell. Subsequently, the lookup  
314 tables within the Noah-MP model (Niu, Fang et al. 2020) were used to assign the relevant  
315 parameters to the corresponding soil and vegetation categories.

### 316 **2.2.2 SMAP L3 Surface Soil Moisture**

317  
318 Since its successful deployment on January 31, 2015, the Soil Moisture Active Passive (SMAP)  
319 observatory has consistently provided global volumetric soil moisture estimates every two or three  
320 days (Entekhabi, Njoku et al. 2010). Its onboard radiometer, operating in the L-band frequency of  
321 the microwave spectrum, senses the top five centimeters of the soil column. In this study, we  
322 selected the SMAP Level 3 morning overpass due to the greater likelihood of air and surface  
323 temperature equilibrium during these hours, a critical condition for the SMAP retrieval algorithm.  
324 The L3 SMAP data used here span from 2015 to 2020, have a spatial resolution of 9 kilometers  
325 and are instrumental in calculating SMM across the Continental United States (CONUS).

326  
327 In line with established methodologies from previous research (He et al., 2023; Mccoll et al.,  
328 2019), a quality control protocol was deemed necessary to refine soil moisture data in regions  
329 affected by dense vegetation, bodies of water, and permafrost, thereby mitigating noise present in  
330 satellite measurements (He et al., 2023; Mccoll et al., 2019; McColl, McColl, Wang, et al., 2017).  
331 However, this study is conducted to determine SMM to deepen our knowledge of physical  
332 processes and to get closer to optimal soil hydraulic parametrizations within Noah-MP. This is  
333 achieved through a comparative analysis of SMM derived from SMAP and Noah-MP datasets.  
334 Given that a specific parametrization within Noah-MP has a pronounced impact on the eastern  
335 region of the Continental United States (CONUS)—a region that also corresponds with a  
336 significant portion of SMAP's low-quality data—we chose not to filter SMAP data to fully capture  
337 the parametrization effects within our study's geographical focus. This approach was intended to  
338 maintain consistency across figures and enhance the presentation of our findings. Furthermore, our

339 objective is to showcase the physical process involved in SMM, rather than focusing on model  
340 accuracy in comparison with SMAP data. Note that the SMM maps from McColl et al (2019) and  
341 He et al (2023) demonstrated the effect of removing SMAP low-quality data, and hence we did  
342 not include the map of locations with high-quality SMAP data. Given that the surface water  
343 balance is sensitive to the temporal resolution of the analyzed surface soil moisture data, the SMAP  
344 L3 soil moisture data are resampled to achieve a consistent sampling frequency of one per three  
345 days at each pixel (He et al., 2023; McColl, Wang, et al., 2017). To ensure the comparability, the  
346 Noah-MP modeled soil moisture data were selected to correspond to the SMAP observation times.  
347 This alignment minimizes potential biases introduced by temporal differences and facilitates a  
348 consistent analysis of soil moisture memory. It is important to note that the sampling frequency,  
349 as highlighted by Shellito et al. (2016), can significantly influence the computation of  $\tau_L$ . This  
350 potential impact was mitigated in this study by aligning the Noah-MP data with SMAP observation  
351 times and maintaining a consistent sampling frequency of one observation every three days,  
352 thereby ensuring the reliability of SMM analysis.

353  
354  
355  
356

### 357 2.2.3 International Soil Moisture Network (ISMN)

358  
359 In evaluating the Noah-MP model's parametrization for the root zone soil moisture, SMM is  
360 computed using both the model's outputs and in situ observations across the CONUS. We obtained  
361 the in situ soil moisture data from the International Soil Moisture Network (ISMN) portal (Dorigo,  
362 Wagner et al. 2011), which compiles quality-controlled measurements from various sensors across  
363 multiple networks, Figure 2. We exclude stations with less than 90% of their data rated as “good”  
364 quality. Despite the diversity of sensor types within ISMN, its stringent quality assurance protocols  
365 suggests that it is a reliable benchmark for validating soil moisture products (Shellito, Small et al.  
366 2016, Colliander, Jackson et al. 2017). For the representation of root zone soil moisture, we select  
367 only the data from the top 1 meter of soil flagged as “good” quality. These measurements are  
368 averaged, i.e., hourly data aggregated to daily means, and the daily time series are used to compute  
369 both long-term and short-term SMM. For the root-zone analyses, the Noah-MP outputs were  
370 sampled to ensure the temporal consistency with SMAP surface-layer observation times. Similarly,  
371 ISMN data were resampled to match the SMAP observation times, ensuring the same sampling  
372 frequency across all datasets used as benchmarks for the root-zone SMM analysis.

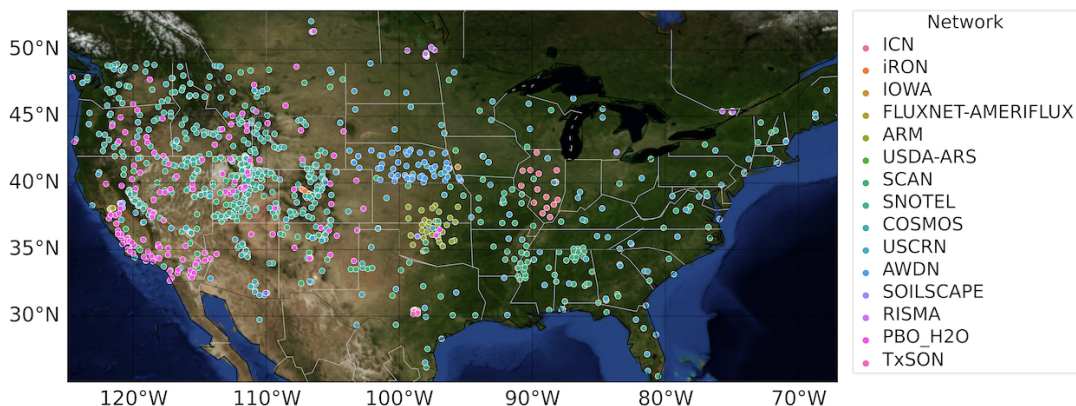


Figure 2 ISMN in-situ locations and networks over CONUS.

373

### 374 **2.3 Noah-MP with Advanced Soil Hydrology**

375

376 In this study, we choose Noah-MP (Niu, Yang et al. 2011, Yang, Niu et al. 2011, Niu, Fang et al.  
377 2024) for its extensive use within the Weather Research and Forecasting (WRF) model, the Unified  
378 Forecast System (UFS) for weather and short-term climate projections, and the National Water  
379 Model (NWM) for streamflow and water resource forecasting. The "semi-tile" sub-grid  
380 methodology of Noah-MP enables detailed calculation of surface energy and fluxes, differentiating  
381 effectively between bare and vegetated terrains to precisely compute variables such as latent and  
382 sensible heat fluxes (Agnihotri, Behrangi et al. 2023).

383

384 The Noah-MP version used in this study includes additional developments in plant hydraulics that  
385 explicitly represent plant water storage supplied by root water uptake driven by the hydraulic  
386 gradient between the soil and roots (Niu et al., 2020) and advanced soil hydrology that solves  
387 mixed-form Richards' equation and thus explicitly represents surface ponding, infiltration of  
388 surface ponded water, and preferential flow (Niu et al, 2024). As such, current Noah-MP accounts  
389 for water flow driven by the hydraulic gradients from the soil to the vegetation canopy to meet the  
390 plant transpiration demand. It also accounts for subgrid variability in infiltration capacity through  
391 a fractional area of preferential flow pathways caused by soil macropores in the fields. A detailed  
392 description of the underlying physical mechanisms for the schemes used in this study can be found  
393 in Niu et al, (2024), also a brief description of equations and parameters is included in supporting  
394 material.

395

396 **The Mixed-Form Richards' Equation:** Most LSMs solve the mass-based (or  $\theta$ -based) Richards'  
397 Equation (RE) for unsaturated soils (Chen and Dudhia 2001, Oleson, Lawrence et al. 2010) and  
398 thus are not adequate to represent saturated conditions, e.g., surface ponding and groundwater  
399 dynamics. The current Noah-MP adopts the methodology of (Celia, Bouloutas et al. 1990) to solve  
400 the mass-pressure ( $\theta$ - $h$ ) mixed-form RE (MF). The new solver solves pressure head,  $h$ , and  
401 conserves mass due to the mass ( $\theta$ ) constraint. To achieve a more accurate solution of  $h$  and mass  
402 balance, the solver takes an adaptive time stepping scheme.

403 Surface ponding occurs when the pressure head of the surface layer is greater than the air entry  
404 pressure, and the upper boundary condition (BC) shifts from flux BC to head BC following  
405 Paniconi (1994). Infiltration-excess runoff occurs when the surface ponding depth,  $H_{top}$ , surpasses  
406 a predefined threshold,  $H_{top,max}$ , at which the surface ponded water at local depressions of a model  
407 grid starts to be connected and runs off. The model extends its vertical domain to the bedrock depth  
408 (Pelletier et al., 2016) at which the lower BC is set up as a zero-flux BC. Groundwater discharge  
409 is simply represented using the TOPMODEL concept as a function of water table depth, which is  
410 determined by the modeled pressure head, which is interpolated between saturated zone and its  
411 overlying unsaturated zone.

412 **Optional Soil Hydraulics Schemes:** The current Noah-MP provides optional hydraulics schemes  
413 of the Van Genuchten-Mualem (VGM) and the Brooks-Corey with Clapp-Hornberger (BC/CH)

414 parameters. To facilitate quicker convergence, particularly near saturation, we smoothed the  
 415 BC/CH water retention curve using a polynomial function following (Bisht, Riley et al. 2018).

416 **Representing Preferential Flow:** To represent preferential flow, current Noah-MP adopts a dual-  
 417 permeability model (DPM) approach, partitioning the model grid into two domains: one  
 418 representing rapid flow with reduced suction head (macropores) and the other for slower matrix  
 419 flow, following Šimůnek & van Genuchten, (2008) and Gerke and van Genuchten (1993a,b, 1996)  
 420 (Gerke and van Genuchten 1993, Gerke and van Genuchten 1993, Gerke and van Genuchten 1996,  
 421 Šimůnek and Van Genuchten 2008). This approach represents subgrid variability in infiltration  
 422 capacity through a fractional area of soil macropores in the fields,  $F_a$ , (or volumetric fraction of  
 423 macropores). DPM also represents water transfer between the two pore domains, which can be  
 424 either be positive (“lateral infiltration” during rainy days) or negative (diffusion from micropores  
 425 to drier macropores). It also accounts for lateral movement of surface ponded water from the matrix  
 426 to macropore domains at the soil surface. The aggregated water content ( $\theta$ ) and vertical water flux  
 427 ( $q$ ) for a grid cell are given by  $\theta = F_a \theta_a + (1-F_a) \theta_i$ , and  $q = F_a q_a + (1-F_a) q_i$ , respectively,  
 428 where  $q$  denotes a water flux and the subscripts  $a$  and  $i$  respectively indicate macropore and  
 429 micropore domains. This approach also extends to other water fluxes, such as direct evaporation  
 430 from soil surface,  $E_{soil}$ , and groundwater recharge.

432 Table 1 Noah-MP Options used in this study.

433

Process	Options	Schemes
Dynamic vegetation	DVEG = 2	Dynamic vegetation
Canopy stomatal resistance	OPT_CRS = 1	Ball-Berry type
Moisture factor for stomatal resistance	OPT_BTR = 1	Plant water stress
Runoff and groundwater	OPT_RUN = 1	TOPMODEL with groundwater
Surface layer exchange coefficient	OPT_SFC = 1	Monin-Obukhov similarity theory (MOST)
Radiation transfer	OPT_RAD = 1	Modified two-stream
Ground snow surface albedo	OPT_ALB = 3	Two-stream radiation scheme (Wang et al., 2022)
Precipitation partitioning	OPT_SNF = 5	Wet bulb temperature (Wang et al., 2019)
Lower boundary condition for soil temperature	OPT_TBOT = 2	2-m air temperature climatology at 8m
Snow/soil temperature time scheme	OPT_STC = 1	Semi-implicit
Surface evaporation resistance	OPT_RSF = 1	Sakaguchi and Zeng (2009)
Root profile	OPT_ROOT = 1	Dynamic root (Niu et al., 2020)

## 434 2.4 Model Experiments

435

436 We conducted five experiments using the current Noah-MP driven by the hourly NLDAS-2 forcing  
 437 data at a spatial resolution of 0.125 degree, starting with the same uniform initial conditions—  
 438 namely, soil moisture at  $0.3 \text{ m}^3\text{m}^{-3}$  and soil temperature at 287K—spanning 2014 to 2019 for six  
 439 iterations. The initial five iterations were dedicated to the model's spin-up phase, and the resulting

440 surface and root zone soil moisture from the last iteration were used for SMM analysis. Parameters  
441 were adopted per the updates by Niu et al. (2020), with adjustments to the dynamic vegetation  
442 module to align with Moderate Resolution Imaging Spectroradiometer (MODIS) leaf area index  
443 observations. This study refrained from parameter calibration related to dual-domain schemes for  
444 preferential flow (Šimůnek and Van Genuchten 2008) and ponding depth.

445  
446 The five experiments are conducted with Noah-MP configurations with different water retention  
447 and infiltration schemes. Table 1 lists optional schemes that were the same for all these  
448 experiments. For other processes, including surface layer turbulent exchange, radiation transfer,  
449 phase changes between snow and rain, and the permeability of frozen soil. For this study, we  
450 selected only those schemes that have a direct impact on the simulation of soil moisture dynamics  
451 (as detailed in Table 2). All these experiments are set with the same number of soil layers, which  
452 vary spatially from 5 – 15 vertical layers with fixed layer thicknesses:  $\Delta z_i = 0.05, 0.3, 0.6, 1.0, 2.0,$   
453  $2.0, 4.0, 4.0, 5.0, 5.0, 5.0, 5.0, 5.0, 5.0, 5.0,$  and 5.0 m down to 49.0 m to match the maximum bedrock  
454 depth data of Pelletier et al. (2016) with a minimum bedrock depth of 4.0 m. The model was  
455 customized using a combination of three soil moisture solver variants, two soil hydraulics schemes,  
456 and two ponding depth thresholds.

457  
458 To explore the influence of surface ponding on SMM, we designed two distinct experimental  
459 conditions. The first condition, designated as MF\_VGM0, excluded the ponding effect by setting  
460  $H_{top,max}$  to 0 mm. Conversely, the second condition, identified as MF\_VGM200, incorporated a  
461 significant ponding depth of 200 mm. Both conditions utilized the mixed-form RE solver alongside  
462 the Van-Genuchten (VGM) model (refer to Table 2). Furthermore, we conducted comparative  
463 analyses to assess the role of soil hydraulic properties by conducting experiments with the Brooks-  
464 Corey/Clapp-Hornberger (BC/CH) model (MF\_CH) and the VGM model (MF\_VGM), each with  
465 a ponding depth threshold of  $H_{top,max} = 50$  mm.

466 An additional experiment employs the Dual-Permeability model (DPM) within the VGM  
467 framework, maintaining the same ponding threshold of  $H_{top,max} = 50$  mm, referred to as  
468 DPM\_VGM (see Table 2). The comparison of DPM\_VGM with the MF\_VGM setup aimed to  
469 shed light on the effects of preferential flow channels on soil moisture forecasting, and runoff  
470 forecasting in future studies, thereby enhancing our comprehension of the complexities inherent  
471 in hydrological modeling.

472  
473 To define the macropore volume fraction, we used the modeled Soil Organic Matter (SOM), which  
474 is computed from Noah-MP with a microbial-enzyme model (Zhang, Niu et al. 2014) prior to the  
475 major experiments conducted in this study through a long-term (120 years) spin-up simulation  
476 from 1980 – 2019 driven by the NLDAS data. The modeled SOM shows a pattern of less SOM in  
477 wet regions but more in arid regions due to more active microbial activities (decomposition and  
478 respiration) in wetter regions. The resulting macropore volume fraction ranges from 0.05 – 0.15  
479 changing with spatially-varying SOM. While we conducted sensitivity analyses on key parameters  
480 such as the ponding depth threshold and macropore fraction to identify ranges yielding realistic  
481 outcomes, we acknowledge that further model development (building relationships with global  
482 high-resolution DEM and soil data, e.g., SoilGrids250m (Poggio, de Sousa et al. 2021) are  
483 necessary to refine the parameters.

484  
485 Table 2 Model experiment configuration.

Experiment ID	Models	$H_{top,max}$ (mm)	Soil Hydraulics
MF_VGM0	Mixed Form RE	0	Van-Genuchten
MF_VGM200	Mixed Form RE	200	Van-Genuchten
MF_CH	Mixed Form RE	50	Brooks-Corey/Clapp-Hornberger
MF_VGM	Mixed Form RE	50	Van-Genuchten
DPM_VGM	DPM	50	Van-Genuchten

486

### 487 3. Results

488

489 In Sections 2.1 and 2.2 of our study, we focus on computing the SMM for both the surface (5 cm)  
490 and root zone (up to 1m) layers, respectively. This dual-layer analysis is fundamental to our  
491 experiments as it allows us to understand the differential impacts of various parameterizations on  
492 soil moisture. By comparing and analyzing the SMM values across these two distinct layers, we  
493 can identify specific physical processes that influence soil moisture dynamics. This comparative  
494 approach not only elucidates how these processes affect SMM but also helps in understanding the  
495 interaction between surface characteristics and subsurface moisture dynamics, which are critical  
496 for improving hydrological modeling and prediction.

497

#### 498 3.1 Long- and Short-Term Soil Moisture Memory of the Surface Layer

499

500 Figure 3 illustrates the spatial distribution of median long-term memory, derived from the five-  
501 year soil moisture dataset. We also provide plots for the SMM spatial distributions to offer insights  
502 for each model experiments. However, it turns out that interpreting the fundamental mechanisms  
503 behind the distribution is very challenging regarding the spatial distributions of other controlling  
504 factors, e.g., climatic forcing, vegetation/soil type, elevation, slope angle/aspect (affecting solar  
505 radiation), which directly or indirectly controls actual ET and runoff as well as interactions  
506 between ET and soil moisture (Rahmati et al., 2024). As such, we focus on comparing the median  
507 SMM values across model scenarios to find the dominate hydrological processes controlling  
508 SMM, because the modeled distributions from the different experiments generally show the same  
509 shape, especially for the same hydraulics (e.g., VGM). Analysis of the SMAP data revealed that  
510 long-term memory ( $\tau_L$ ) is significantly higher in the energy-limited and humid regions of the  
511 eastern US, and lower in the arid western regions. These findings are consistent with those of He  
512 et al. (2023) and McColl et al. (2019).

513

514 The MF\_CH experiment displays a spatial pattern that contrasts with the SMAP data, with a longer  
515 memory in the arid western regions but a shorter memory in the wet northeastern regions (Figure  
516 3a & 3b). This is likely caused by the faster drainage of topsoil water under the wetter conditions,  
517 whereas under the drier conditions, the spuriously stronger suction from the CH hydraulics sustain  
518 the surface soil moisture for a longer period. Further examination reveals that models using the  
519 Van-Genuchten scheme reflect SMAP's patterns. Specifically, the eastern regions display higher  
520  $\tau_L$  values, while the western regions show lower values (see Figure 3b-f). DMP\_VGM  
521 demonstrates a shorter memory in the eastern CONUS compared to MF\_VGM (refer to Figures

522 3c, d, and S1. VGM scenario with zero ponding depth shows a shorter memory compared with  
 523 MF\_VGM200 in the eastern CONUS (Figures 3e and f), where surface ponding happens more  
 524 frequently and with a greater depth. Figure S2 shows a better match of data points with the  
 525 agreement line in the DPM\_VGM versus SMAP scatterplot. In contrast, the MF\_CH versus SMAP  
 526 scatterplot lacks this alignment with a correlation of  $-0.10$ . The correlation values have risen from  
 527  $-0.10$  to  $0.15$  with VGM, a sign of progress, but they are still not strong.  
 528  
 529  
 530

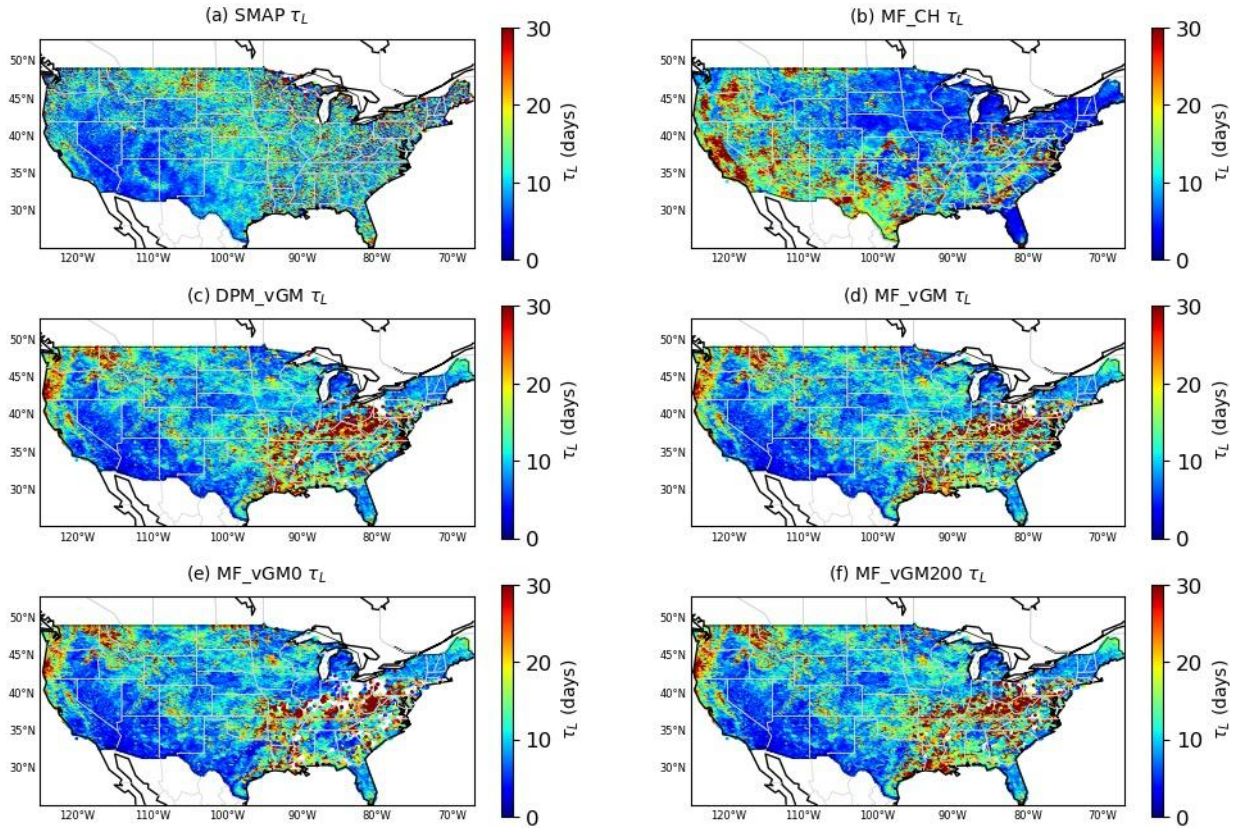


Figure 3. Long-term SMM derived from various datasets from 2015 – 2019 for soil surface layer: (a) SMAP; (b) MF\_CH; (c) DPM\_VGM; (d) MF\_VGM; (e) MF\_VGM0; and (f) MF\_VGM200. SMM = Soil Moisture Memory

531  
 532 To assess the influence of plant water storage on SMAP soil moisture data and the resultant SMM,  
 533 we employed the MODIS NDVI to categorize the entire CONUS into wet ( $NDVI > 0.45$ ) and dry  
 534 regions ( $NDVI < 0.45$ ). In the dry areas (see Figure 4a), the probability distribution function (PDF)  
 535 of the surface SMM from MF\_CH differs from that of SMAP and exhibits a higher median of  
 536 10.53 days compared to SMAP's 8.47 days (overestimation). Other model scenarios using van  
 537 Genuchten (VG) hydraulics, with an SMM median of around 8.6 days, show a distribution PDF  
 538 like SMAP. Note that the VGM scenarios effectively tackle the problem of long-term memory  
 539 overestimation, a point emphasized by He et al. (2023). This improvement is due to the refined  
 540 parametrization of physical processes within the VGM experiments.

541

542 In the wet regions with dense vegetation (Figure 4b), the SMM PDF of MF\_CH (median of 8.03  
543 days) significantly varies from the SMAP PDF (median of 10.71 days), showing an  
544 underestimation of  $\tau_L$ . However, due to the strong effect of plant water storage on the SMAP's soil  
545 moisture retrieval (commonly in the eastern CONUS), our focus here is on model sensitivity to  
546 process representations rather than on model accuracy relative to SMAP data. Other models with  
547 the van Genuchten (VG) scheme display greater variability among themselves in wet areas (Figure  
548 4b) than in the dry region (Figure 4a). MF\_VGM0 (with a zero ponding depth threshold) shows a  
549 shorter long-term SMM, with a median of 10.72 days, compared to MF\_VGM200 (with a 200 mm  
550 threshold), with median of 12.05 days, and MF\_VGM (with 50 mm ponding threshold), with a  
551 median of 12.03. This suggests extra water inputs from the surface ponded water (MF\_VGM200)  
552 can help extend the surface SMM. Changing the ponding depth threshold from 50 mm (MF\_VGM)  
553 to 200 mm (MF\_vGM200), has a marginal effect on  $\tau_L$ , suggesting that the response does not  
554 proportionally increase with higher values. With the same 50 mm ponding threshold, DPM\_VGM  
555 produces a shorter SMM, with a median of 11.73 days, than MF\_VGM, indicating that the effects  
556 of faster water drainage of the topsoil water caused by the preferential flow (as represented by  
557 DPM\_VGM) can last longer.

558

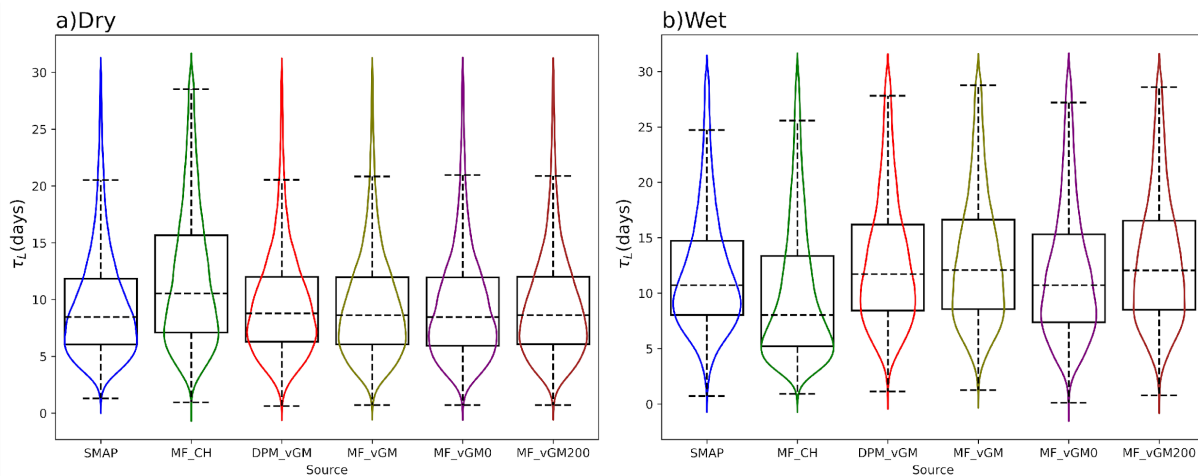


Figure 4 Violin plot of surface  $\tau_L$  estimated from SMAP and Noah-MP scenarios for dry regions with less vegetation (NDVI < 0.45) and wet regions with more vegetation (NDVI > 0.45).

559

560 For the short-term SMM, all the scenarios produce an overall spatial pattern similar to that of the  
561 SMAP-derived  $\tau_s$ , showing a longer memory in the drier western US than in the wetter eastern  
562 (Figure 5). However, MF\_CH shows a shorter memory in the northwestern US than that derived  
563 from SMAP (Figure 5a & b). MF\_CH with a median of 1.9 days underestimates SMAP with a  
564 median of 2.02 days, while VG scenarios have median  $\tau_s$  around 2.09 days over dry regions. This  
565 effectively rectifies the underestimation in short-term memory by LSMs, as reported in previous  
566 studies (He et al., 2023). He et al. (2023) highlighted that most LSMs tend to underestimate  $\tau_s$ ,  
567 which is strongly affected by soil water drainage as specified by McColl et al. (2019). Note that  
568 higher  $\tau_s$  values indicate slow drainage, whereas lower values suggest faster drainage; this is  
569 exemplified by Figure 5a, which exposes a more rapid drainage in the eastern CONUS in contrast  
570 to the western. The incorporation of surface ponding and DPM (2.08 days) has shown less effects



571 on short-term memory than the soil hydraulics for the dry region (more macropores are available  
572 in wet regions and hence DPM would have more effect in those regions). The introduction of  
573 surface ponding (comparing MF\_VGM0 (2.11 days) to MF\_VGM200 (2.108 days) in Figure 5  
574 and Figure 6) contributes to more persistent surface soil moisture and a bit faster drainage. The  
575 pdf of SMM from all the VGM models more closely resembles the SMAP pdf in the western  
576 United States than in the eastern part of the country due likely to that the SMAP soil moisture  
577 retrieval may be affected by the plant water storage and thus the spatial variations in canopy  
578 density.

579

580 For wet regions, MF\_CH with a median of 1.26 days underestimate SMAP with a median of 1.56  
581 days. DPM\_VGM with faster drainage of surface soil water produces a median  $\tau_s$  of 1.43, shorter  
582 than does MF\_VGM with a median of 1.48 days. The DPM model accelerates the drainage of  
583 water from the topsoil. This effect is more significant in the eastern CONUS. As a result, it lowers  
584 the short-term memory in areas where the soil has macropores.

585

586 The modeling results also indicate the long-term memory of the surface soil moisture is more  
587 sensitive to the four VGM schemes in the wet regions (Figure 4b) than the short-term memory  
588 (Figure 6b). This can be attributed to the differences in how topsoil water responds to surface  
589 ponding and preferential flow as represented by the four VGM across different moisture regimes.  
590 Under higher soil moisture conditions right after a rainfall event, the persistence of soil moisture  
591 is mainly dominated by drainage of topsoil water to deeper soil, whereas at relatively lower soil  
592 moisture, the long-term memory is more controlled by persistent water inputs from surface ponded  
593 water and prolonged drainage by preferential flow. This also indicates that the effects infiltration  
594 of surface ponded water and preferential flow can last longer up to more than 10 days. Under dry  
595 conditions (Figure 4a and 6a), these hydrological processes become less important. However, the  
596 soil water retention curves as represented by the CH and VG schemes play a more important role  
597 under any conditions (Figure 4a and Figure 6a). Another possible reason can be the issue of time  
598 scale. Short-term memory has values up to 5 days, and given the SMAP revisit time of 3 days,  
599 generating values for intervals shorter than 3 days may challenge the validity of short-term  
600 memory as a reliable measurement for soil drainage, as demonstrated by McColl et al. (2019).  
601 Since we selected Noah-MP days corresponding to the SMAP revisit time, it is possible that the  
602 effects of different VG parameterizations were diminished by this sampling. We suggest that other  
603 measurements, such as streamflow and baseflow analysis, should be considered to better quantify  
604 the effect of soil hydraulics on soil drainage (Farmani, Tavakoly et al. 2024).

605

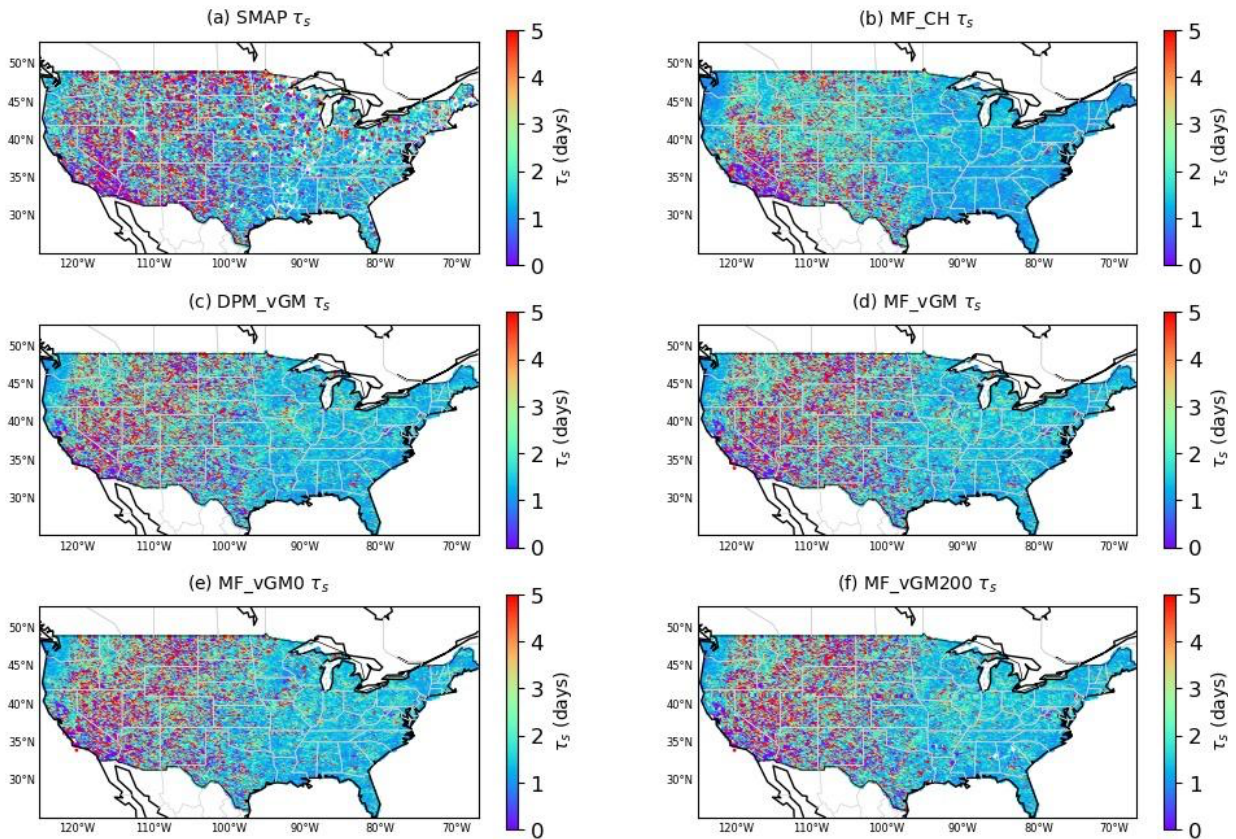


Figure 5 Short-term SMM derived from various datasets from 2015 – 2019 for soil surface layer: (a) SMAP; (b) MF\_CH; (c) DPM\_vGM; (d) MF\_vGM; (e) MF\_vGM0; and (f) MF\_vGM200. SMM = Soil Moisture Memory.

606

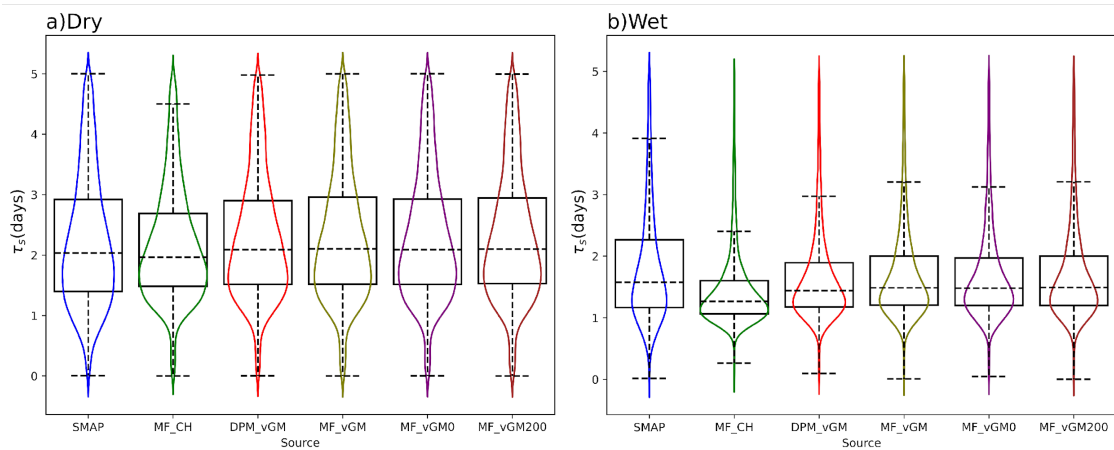


Figure 6 Same as Figure 4 for short-term memory.

607

### 608 3.2 Long- and Short-Term Soil Moisture Memory of the Root Zone Layers

609

610 We use the International Soil Moisture Network (ISMN) soil moisture dataset as the benchmark  
 611 and compute SMM at the ISMN stations as illustrated in Figure 2. We compute the long-term  
 612 SMM across 654 sites within CONUS for the period from 2015 – 2019. The median values of  
 613 these computations indicate that the root zone SMM (Figure 7 & Figure 9) is generally higher than  
 614 the surface SMM (Figure 3 & Figure 5). Analysis of ISMN data reveals that the root zone  $\tau_L$  (Figure  
 615 7) generally exceeds surface  $\tau_L$  (Figure 3), particularly longer in the western US. Some eastern  
 616 locations also exhibit longer  $\tau_L$ , whereas the central region demonstrates lower values.

617  
 618 MF\_CH produces a shorter root-zone  $\tau_L$  across nearly all the sites in CONUS (Figure 7 & Figure  
 619 8). The Van-Genuchten scheme mirrors the ISMN-derived  $\tau_L$ , albeit with slightly higher values  
 620 (Figure 7 & Figure 8). An increase in surface ponding depth raises the  $\tau_L$ . This is particularly true  
 621 in the eastern US, where surface ponding occurs more often, and its impact on soil moisture is  
 622 more substantial. Figures S3 and S4 illustrate this effect. Additionally, DPM\_VGM (Figure 7c and  
 623 Figure 8) reduces the root-zone long-term SMM across most of CONUS relative to the other  
 624 models (Figure 7c, d, e, & f and Figure S3).

625

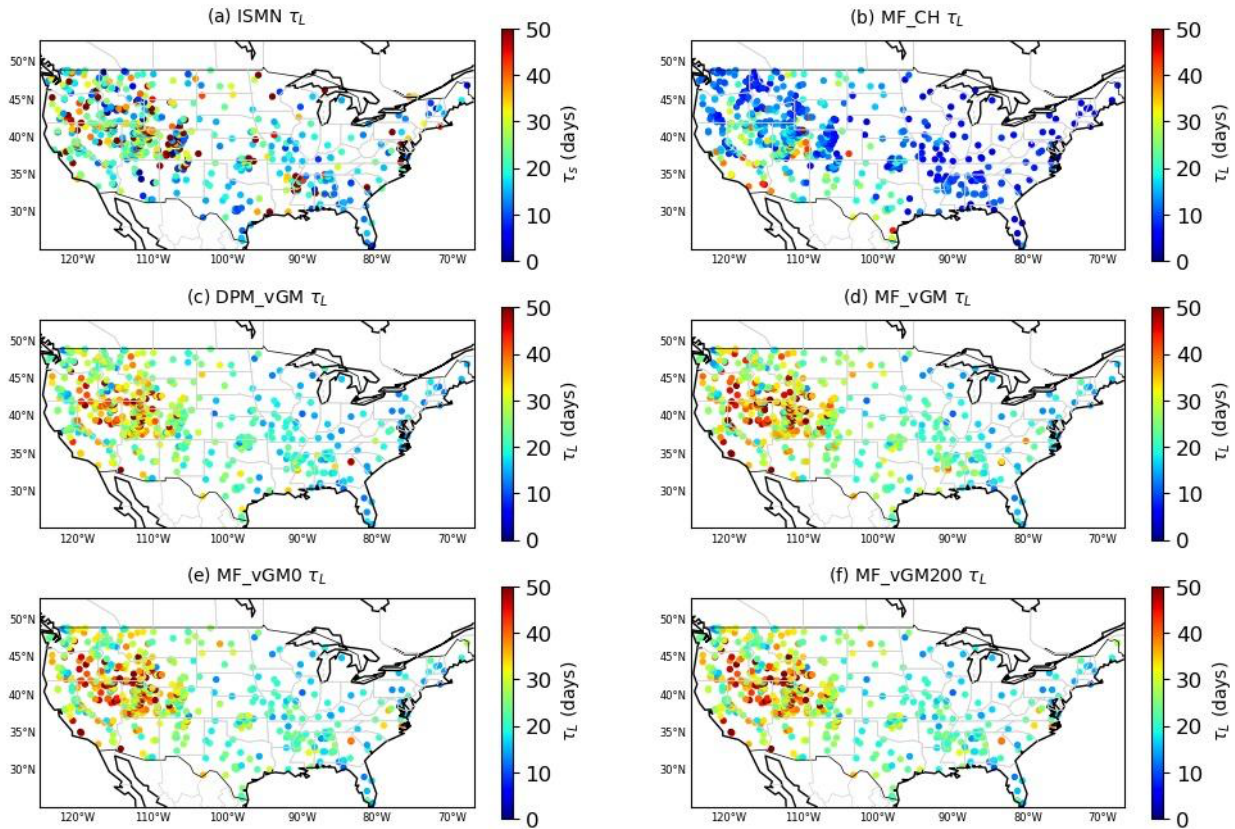


Figure 7 Long-term root-zone SMM derived from various datasets from 2015 – 2019: (a) ISMN; (b) MF\_CH; (c) DPM\_VGM; (d) MF\_VGM; (e) MF\_VGM0; and (f) MF\_VGM200. SMM = Soil Moisture Memory.

626  
 627

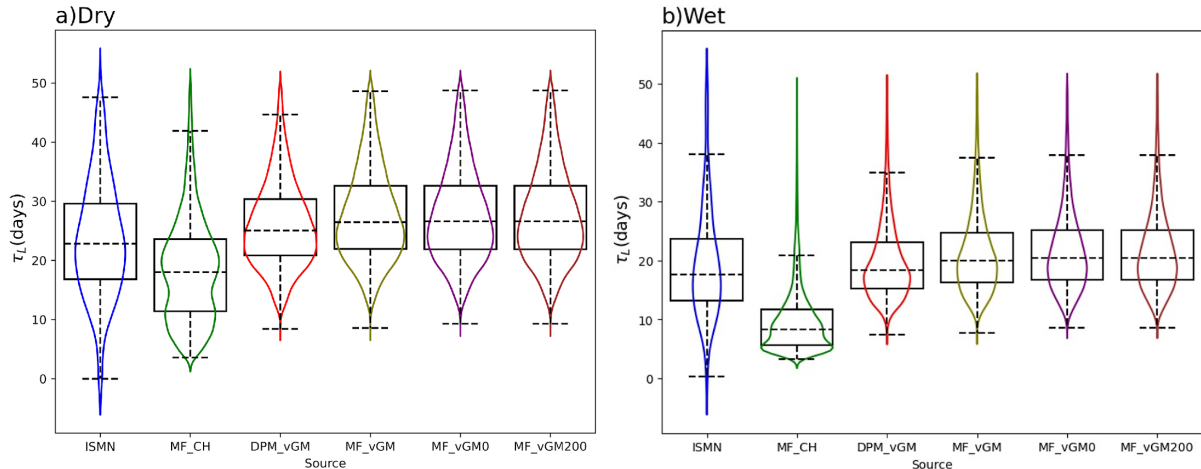


Figure 8 Violin plot of root zone  $\tau_L$  estimated from ISMN and Noah-MP scenarios for dry regions with less vegetation ( $NDVI < 0.45$ ) and wet regions with more vegetation ( $NDVI > 0.45$ ).

628 As for the surface layer, we use the MODIS NDVI to classify all the stations into wet and dry  
 629 regions. In the dry regions (Figure 8a), MF\_CH has a different probability distribution function,  
 630 and a lower median of 19 days compared to that of ISMN (median of 23 days). All the other  
 631 scenarios using VG schemes exhibit a similar SMM PDF to each other, yet they are somewhat  
 632 different from the one derived from ISMN. Also, the presence of macropores reduces long-term  
 633 SMM, with a median of 25 days, and results in the closest median to the ISMN (Figure 8a). ISMN,  
 634 however, shows a large range of long-term SMM compared with all the Noah-MP experiments,  
 635 indicating the complex nature of the observed SMM needs further investigation (Figure 8a & b).  
 636 Note that the analyses were conducted at a limited number of locations, presenting challenges in  
 637 fully capturing the impacts of different parameterizations on SMM.

638

639 In the wet regions, MF\_CH shows smaller  $\tau_L$  values (median of 9.8 days) than that from ISMN  
 640 (median of 18 days) together with a noticeable pdf difference. The effect of dual permeability  
 641 decreases the soil moisture and long-term memory compared with the other model experiments,  
 642 resulting in a median (19 days) close to ISMN (18 days), Figure 8b. However, it seems that the  
 643 ponding depth does not show a noticeable impact on  $\tau_L$ . It should be noted that the effect of ponding  
 644 depth, which slightly increases the long-term memory in RTZ, can be observed in Figure S3 and  
 645 Figure S4 when we take a close look into them.

646

647 Further investigation reveals an enhancement in the model's ability to capture soil hydraulic  
 648 dynamics when shifting from the Clapp-Hornberger to the Van-Genuchten scheme, with an  
 649 improvement in  $\tau_L$  values from 0.05 to 0.12 (Figure S5). Also, The Dual Permeability model with  
 650 Van-Genuchten (DPM\_VGM) demonstrates superior performance with a correlation of 0.15,  
 651 compared to all other scenarios tested.

652

653

654

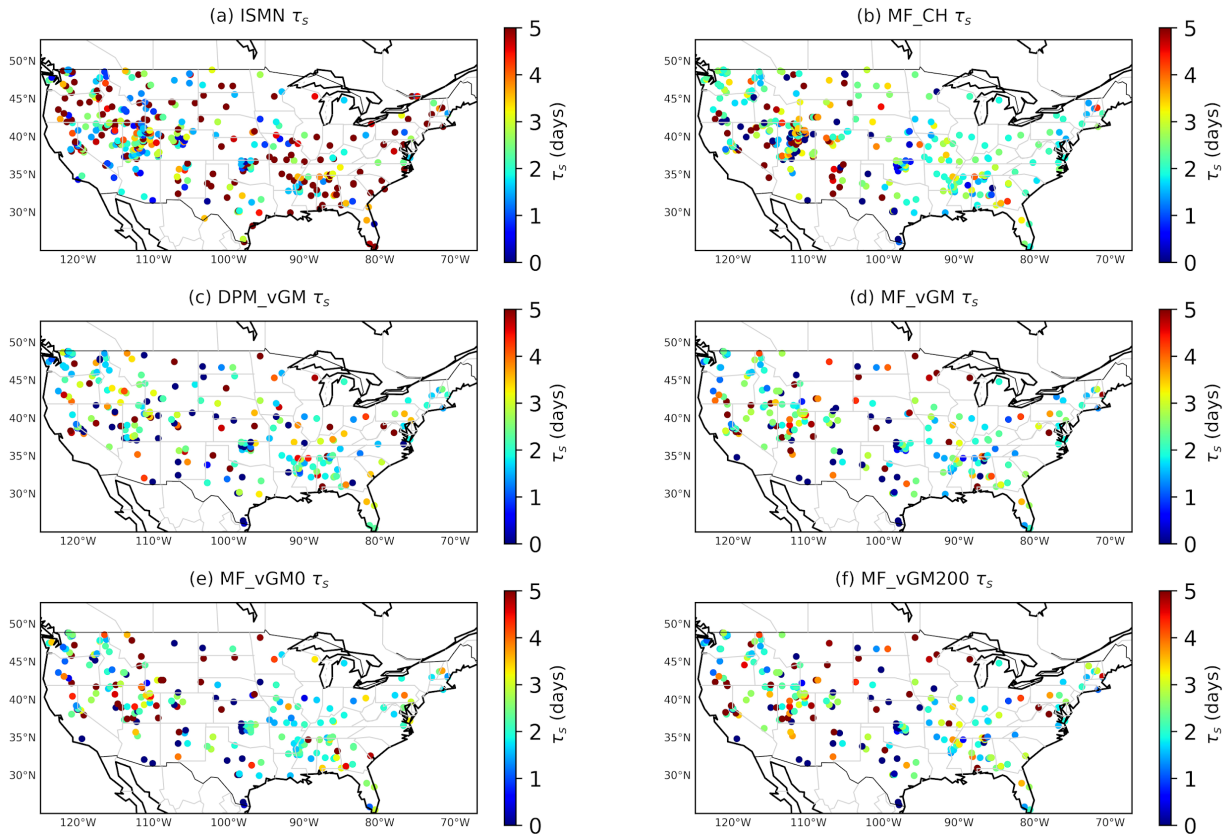


Figure 9 Same as Figure 7 but for short-term.

655

656 The findings show that  $\tau_s$  in most Noah-MP scenarios are comparable to those observed in the  
 657 ISMN data, as shown in Figure 9b to f. However, there is a consistent underestimation in some  
 658 eastern locations. Figure 10 highlights this pattern, showing that wet regions tend to underestimate  
 659  $\tau_s$ , with ISMN reporting a median of 2.5 days and Noah-MP experiments a median of around 2  
 660 days. Conversely, dry regions tend to overestimate, with ISMN at a median of 2.1 days and Noah-MP  
 661 experiments at approximately 2.7 days.

662

663 Although distinguishing between MF\_VGM0 and MF\_VGM200 in Figure 9 and Figure 10 is  
 664 challenging, Figure 11 (Figure 11c and d) reveals that an increase in ponding depth leads to a slight  
 665 decrease in short-term memory in the eastern CONUS. Comparing Figure 9 with Figure 11  
 666 indicates that ISMN stations partially reflect the spatial pattern of long-term and short-term  
 667 memory in the root zone across CONUS. It may be concluded that the spatial patterns of long-  
 668 term and short-term memory (Figure 11 and Figure S7) of the root zone are quite similar to those  
 669 of the surface layer (Figure 3 and Figure 5). Hence, long-term memory is more prevalent in the  
 670 eastern CONUS and mountainous areas, while longer short-term memory occurs predominantly  
 671 in western areas. However, this conclusion is not totally true and further investigation is needed.

672

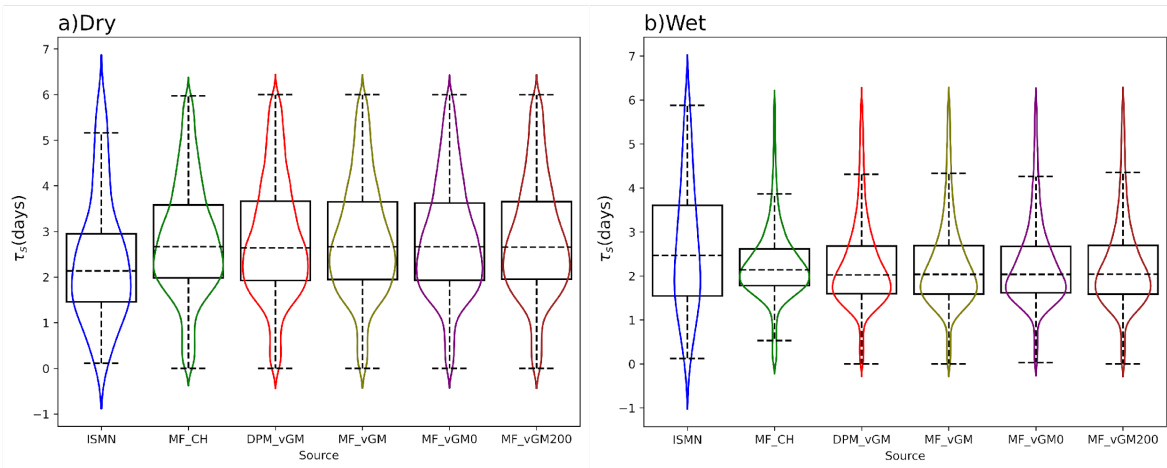


Figure 10 Same as Figure 8 but for the short-term SSM.

673  
674

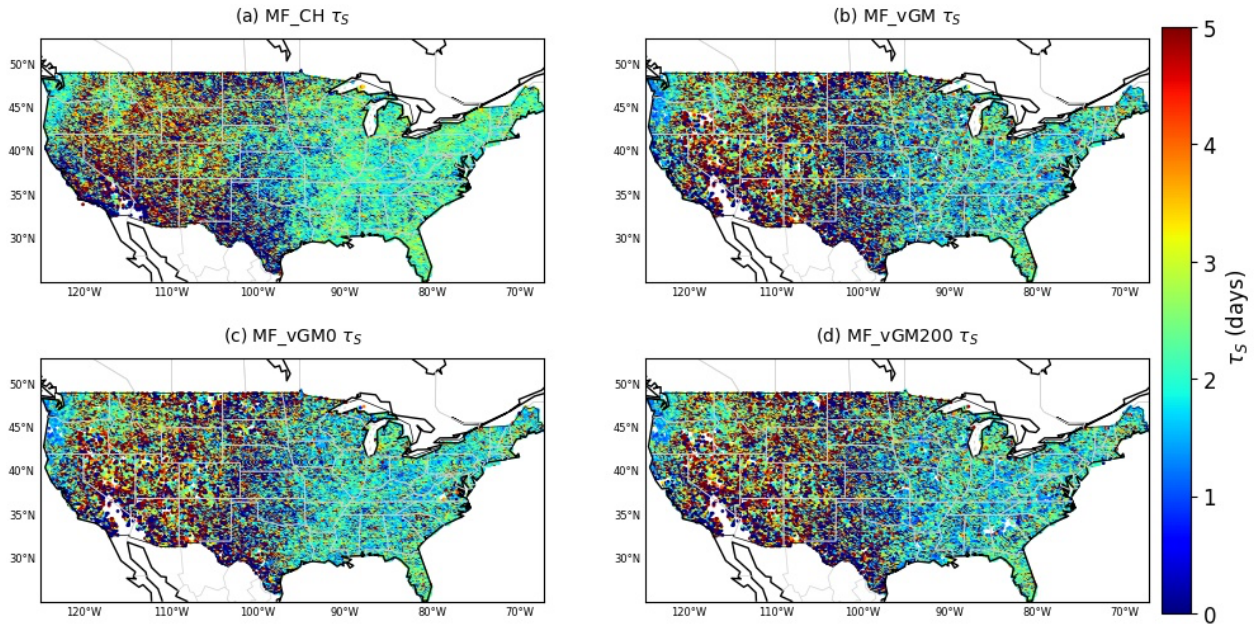


Figure 11 Spatial distribution of root zone  $\tau_s$  estimated from (a) MF\_CH; (b) MF\_vGM; (c) MF\_vGM0; and (d) MF\_vGM200.

675 **4. Discussion**

676 **4.1 How Do Different Parametrizations Affect SMM?**

677  
678 The efficacy of LSMs in simulating climate feedback mechanisms critically depends on the soil's  
679 ability to retain moisture and how fast the soil releases the moisture up to the atmosphere through  
680 soil surface evaporation and plant transpiration and down to the aquifers through recharge. The  
681 rapid infiltration of incident water (rainfall and snowmelt) into deeper subsoil strata reduces the  
682 soil's capacity to return moisture to the atmosphere through evaporation and transpiration. Thereby

683 disrupting potential atmospheric feedback loops in LSMs (Mccoll et al., 2019). Conversely, If  
684 LSMs lose water too quickly through ET, they provide feedback to the atmosphere faster than they  
685 should. Thus, the concept of SMM becomes essential in LSMs, as it can provide information about  
686 the rate at which moisture disappears from soil. Hence, understanding the effects of various  
687 physical processes on SMM is vital for enhancing the representation of these processes in LSMs,  
688 thereby improving their overall performance in simulating the complex interactions between the  
689 land surface and the atmosphere.

690

691 The water retention curve characteristics of the BC/CH hydraulics scheme are characterized by a  
692 strong suction force that is more pronounced than in the Van-Genuchten model for various soil  
693 types (Niu et al, 2024). This stronger suction promotes moisture transfer from the deeper layers to  
694 the surface layer, causing the surface soil to retain more moisture (Figure S6) and has a longer  $\tau_L$   
695 (Figure 3, 4), a common issue in LSMs according to He et al. (2023). Moreover, the higher suction  
696 reduces the root zone moisture and consequently, it would have a shorter  $\tau_L$  (Figure 7 and 8).  
697 Conversely, the VG scheme, with weaker suction, transfers less moisture from the root zone to the  
698 surface, resulting in a drier surface layer and a shorter  $\tau_L$  for the surface, but a longer  $\tau_L$  for the root  
699 zone, as depicted in Figures 7 and 8.

700

701 Short-term memory is inversely related to moisture availability; thus, a wetter soil has a shorter  $\tau_S$ ,  
702 whereas a drier layer has a longer  $\tau_S$ . The VG scheme produces a drier surface layer and a moister  
703 root zone, leading to a longer surface  $\tau_S$  but a shorter root zone  $\tau_S$  compared to the BC/CH scheme,  
704 as shown in Figures 5, 6, and 11.

705

706 As indicated in a previous study (He et al., 2023), a common issue in LSMs is the overestimation  
707 of the long-term memory of surface soil over dry regions. This could be attributed to  
708 underestimation of evaporation within LSMs using the CH parametrization (Figure S7a), resulting  
709 in overestimation of soil moisture. However, a shift towards the VG scheme increases the  
710 evaporation (Figure S7b, Figure S8), and hence it overcomes the  $\tau_L$  overestimation (Figure 3 and  
711 4).

712

713 The presence of soil macropores promotes infiltration at the soil surface and rapid flow through  
714 preferential pathways from the surface to the root zone (Mohammed et al., 2021), consequently  
715 reducing the moisture retained in the surface layer. Moreover, macropores lead to reduced suction  
716 of the soil, hence less water from subsurface soil was pulled up to the surface, causing the topsoil  
717 to have less moisture (Figure S6). Therefore, macropores lead to a decrease of surface  $\tau_L$ (Figure  
718 3d, 4b). Moreover, the presence of macropores increases the root-zone soil moisture and  
719 consequently, it should prolong the root zone  $\tau_L$ . However, the even distribution of macropores  
720 throughout the soil profile in current Noah-MP configuration, DPM\_VGM, increases water  
721 infiltration into deeper layers, resulting in faster flow to deep soil layers, recharge to groundwater  
722 and thus a drier root zone. As a result, macropores reduce the root-zone long-term SMM (Figure  
723 7d, e, & f and Figure S8) of DPM\_VGM. This highlights the importance of calibration of  
724 macropore profile in DPM\_VGM for better representations of macropore effects and soil  
725 hydrohalic dynamics.

726

727 While the soil matrix typically allows for only slow water movement due to the pressure gradient,  
728 macropores enable rapid gravitational flow (Mohammed et al., 2018). These macropores facilitate

729 quicker infiltration to the root zone (Mohammed et al., 2021). Therefore, they increase the drainage  
730 rate to these deeper layers, which slightly reduces the short-term soil moisture memory in the  
731 surface (Figures 5 and 6). Additionally, as water moves from the surface to the root zone, the  
732 increased moisture content there leads to quicker drainage (we speculate that this occurs in the real  
733 world; however, in the current DPM\_VGM, the deep soil is wetter than root zone, indicating a  
734 need for calibration of the macropore profile as we have stated). Consequently, this process further  
735 decreases the short-term moisture memory in the root zone due to the higher drainage rates of  
736 wetter soil.

737

738 Finally, the ponding threshold allows water to remain on the surface before turning into runoff.  
739 This provides water with more time to percolate into the soil. The consequent increase in ponding  
740 depth allows extended water infiltration, thus enhancing soil moisture and lengthening moisture  
741 retention through the soil profile (Figure S6e, f). So as discussed before, wetter soil leads to  
742 prolonged  $\tau_L$  and shorten  $\tau_S$  (Figure 5, 6, 7, 11).

743

#### 744 **4.2 Limitation of Our Study**

745

746 Some sources of uncertainty may affect our results in this study, including uncertainties in input  
747 data, and models. The SMAP L-band penetration depth can indeed be shallower than 5 cm,  
748 especially over wetter regions like the eastern CONUS, which may introduce a mismatch when  
749 comparing SMAP observations with the Noah-MP 5 cm layer. SMAP reliability is affected by  
750 plant water storage change (in the eastern part and some mountainous sites), introducing  
751 uncertainties into SMM values for the benchmark. While SMAP observations may be less reliable  
752 over these densely vegetated areas, they still support our objective of enhancing our understanding  
753 of the physical processes in soil hydrology. Furthermore, the SMM patterns captured from SMAP  
754 can be insightful in understanding regional variabilities in SMM.

755

756 Another concern is the influence of ISMN spatial representation on SMM analysis. ISMN stations  
757 are point-based, and it is assumed that one point represents a 1/8-degree grid area. It is possible  
758 that the point measurements cannot fully capture the spatial variability within the Noah-MP grid  
759 cells, leading to discrepancies in the representation of values and spatial patterns. The limited  
760 number of stations may further amplify this issue. One potential solution to address the scale  
761 mismatch between point-based observations and grid-scale simulations is the use of high-  
762 resolution or hyper-resolution models. These models can provide finer spatial detail, allowing for  
763 a more direct comparison between observational data and model outputs, thereby improving the  
764 accuracy of the analysis and reducing scale-induced biases. Incorporating such approaches in  
765 future studies would help mitigate the limitations posed by the current scale differences.

766

767 Additionally, some model representations may require further investigation. The DPM\_VGM  
768 scheme uses a vertically constant macropore volume fraction, which means macropores generated  
769 by biotic factors (formed by wormhole and dead roots) and abiotic factors (cycles of freezing-  
770 thawing and drying-wetting) are fixed down to the bedrock. However, in nature, these macropores  
771 would reduce after a few meters from the soil surface. Because the existence of macropores in  
772 nature drains the surface layer and increases the root zone soil moisture, to better represent the  
773 actual physical process, it is necessary to incorporate more soil data, e.g., the soil organic matter  
774 and coarse materials from e.g., SoilGrid250m (Hengl et al., 2017) for climate predictions or



775 calibrate macropore volume fraction for hydrological applications. Such a calibration is anticipated  
776 to further advance the fidelity of soil moisture simulations, enhancing the model's utility in various  
777 hydrological and climate applications.

778  
779 Concerning surface water ponding, a constant ponding threshold may not be justified, and a  
780 spatially variable surface ponding may lead to improved model accuracy. Future model  
781 developments should consider micro-scale topographic variations to represent the hydrologic  
782 connectivity of surface ponded water. We tested a scheme of ponding threshold as a linear function  
783 of the subgrid standard deviation of DEM derived from DEM at 30 m resolution (although not  
784 enough), resulting larger surface ponding thresholds over the alpine western US. Further  
785 investigation is needed to validate and calibrate the modeled areal ponding fraction and depth  
786 against satellite (or camera) derived. We expect a more realistic representation of ponding  
787 threshold through further calibration of the parameters in the function.

788  
789 There are additional factors, such as water convergence through surface and subsurface lateral  
790 flows (e.g., Barlage et al., 2021), that may affect SMM but are not represented by the current Noah-  
791 MP version and thus not considered in our analysis. The primary focus of our study is to understand  
792 the impacts of missing processes on SMM and use this understanding to guide future LSM  
793 development for S2S climate predictions, for instance, the surface ponding and preferential flow.  
794 Consequently, we narrowed our examination down to key missing processes represented within  
795 Noah-MP. Future research would further evaluate the impact of lateral flows and other processes  
796 on SMM, expanding our understanding of these dynamics and their implications for climate  
797 prediction. Moreover, this study focuses primarily on physical process representations and  
798 parameterizations for soil moisture dynamics, while we acknowledge the strong impacts of  
799 uncertainties in hydraulic parameters.

## 800 **5. Conclusion**

801  
802 In this study, we have explored the effects of soil hydraulic schemes and hydrological processes  
803 on SMM using the Noah-MP LSM with advanced hydrology. Our research was motivated to  
804 understand how missing physical processes help solve the commonly observed biases in long-  
805 term/short-term SMM by LSMs. We aim to find the key missing processes controlling SMM and  
806 thus to improve the representation of soil hydrology in LSMs, using the knowledge gained from  
807 our analysis of SMM. We designed and implemented five scenarios to focus on the impacts of key  
808 missing processes and different hydraulic parametrizations. These scenarios include two soil  
809 hydraulic models (Clapp and Hornberger and Van-Genuchten), a dual permeability model  
810 representing preferential flow, and three surface ponding thresholds. Using soil moisture datasets  
811 from SMAP and ISMN for surface and root zone measurements, respectively, we conducted a  
812 comprehensive analysis of the effects of different Noah-MP parameterizations on soil moisture  
813 memory.

814  
815 Our findings suggest that the soil water retention curve is the most important factor controlling  
816 SMM, due to its strong influence on soil water persistence through suction by the soil particles.  
817 We show that the adoption of the Van-Genuchten parameterization considerably mitigates the  
818 long-standing issue of overestimating SMM in LSMs employing the Brooks-Corey/Clapp-  
819 Hornberger (BC/CH) hydraulic model. The Van-Genuchten model, with its reduced suction effect

820 attributable to a drier surface layer, leads to a more accurate depiction of moisture transfer from  
821 the root zone to the surface, which is important for more realistic description of soil moisture  
822 dynamics.

823  
824 Moreover, representing surface ponding processes allows for an extended period of soil water  
825 infiltration, thus extending both surface and root-zone long-term memories and reducing the short-  
826 term memory. Implementing a dual-permeability approach fine-tunes soil moisture representation  
827 by accounting for preferential flow paths, marking a step forward in the enhancement of soil  
828 moisture memory and the overall fidelity of hydrological simulations. Macropores lead to a  
829 decrease in short-term memory and long-term memory, due to faster drainage and thus decreased  
830 surface soil moisture. Given these compelling advancements, we strongly recommend that LSMs  
831 adopt the VG hydraulics to advance the prediction of hydrological and climatic phenomena.

832  
833 The findings from this study have important implications for future research on SMM. By  
834 identifying the specific parameterizations that lead to discrepancies in long-term and short-term  
835 SMM, future studies should focus on refining these parameters to reduce biases in LSMs.  
836 Moreover, while this study focuses on the effect of the missing hydrological processes on the  
837 timescale of SMM, future research should analyze the impact of these parameterizations on the  
838 strength and legacy of SMM and assess whether the findings based on timescale align with those  
839 related to strength and legacy (Rahmati et al., 2024).

840  
841  
842  
843

#### 844 **Competing interests**

845  
846 The contact author has declared that none of the authors has any competing interests.

#### 847 **Acknowledgments**

848  
849 Funding for this project was provided by the National Oceanic and Atmospheric Administration (NOAA), awarded to  
850 the Cooperative Institute for Research on Hydrology (CIROH) through the NOAA Cooperative Agreement with The  
851 University of Alabama, NA22NWS4320003. Also, the research carried out for this article was supported by the U.S.  
852 Army Corps of Engineers, Engineer Research and Development Center, Coastal Inlets Research Program via  
853 Congressionally Directed R&D with the National Oceanic and Atmospheric Administration's National Water Center.  
854 The data used in this study are freely available online:  
855 NLDAS-2 data (<http://www.emc.ncep.noaa.gov/mmb/nldas/>); NASA SMAP soil moisture product  
856 ([https://nsidc.org/data/spl3smp\\_e/versions/6](https://nsidc.org/data/spl3smp_e/versions/6)); GPM IMERG-Final product  
857 ([https://disc.gsfc.nasa.gov/datasets/GPM\\_3IMERGHH\\_06/summary](https://disc.gsfc.nasa.gov/datasets/GPM_3IMERGHH_06/summary)). The Noah-MP code used in this study has  
858 been uploaded to a repository that may be accessed by other researchers  
859 ([https://github.com/mfarmani95/NoahMP\\_Dual](https://github.com/mfarmani95/NoahMP_Dual)).

860  
861  
862

863 **Reference**

- 864 Agnihotri, J., A. Behrangi, A. Tavakoly, M. Geheran, M. A. Farmani and G. Y. Niu (2023). "Higher Frozen Soil  
865 Permeability Represented in a Hydrological Model Improves Spring Streamflow Prediction From River Basin to  
866 Continental Scales." Water Resources Research **59**(4).
- 867 Bisht, G., W. J. Riley, G. E. Hammond and D. M. Lorenzetti (2018). "Development and evaluation of a variably  
868 saturated flow model in the global E3SM Land Model (ELM) version 1.0." Geosci. Model Dev. **11**(10): 4085-4102.
- 869 Boone, A. (2004). "The Rhône-Aggregation Land Surface Scheme intercomparison project: An overview." **17**: 187-  
870 208.
- 871 Celia, M. A., E. T. Bouloutas and R. L. Zarba (1990). "A general mass-conservative numerical solution for the  
872 unsaturated flow equation." Water Resources Research **26**(7): 1483-1496.
- 873 Chen, F. and J. Dudhia (2001). "Coupling an Advanced Land Surface–Hydrology Model with the Penn State–  
874 NCAR MM5 Modeling System. Part I: Model Implementation and Sensitivity." Monthly Weather Review **129**(4):  
875 569-585.
- 876 Colliander, A., T. J. Jackson, R. Bindlish, S. Chan, N. Das, S. B. Kim, M. H. Cosh, R. S. Dunbar, L. Dang, L.  
877 Pashaian, J. Asanuma, K. Aida, A. Berg, T. Rowlandson, D. Bosch, T. Caldwell, K. Caylor, D. Goodrich, H. al  
878 Jassar and S. Yueh (2017). "Validation of SMAP surface soil moisture products with core validation sites." Remote  
879 Sensing of Environment **191**: 215-231.
- 880 Delworth, T. and S. Manabe (1989). "The Influence of Soil Wetness on Near-Surface Atmospheric Variability."  
881 Journal of Climate **2**(12): 1447-1462.
- 882 Dirmeyer, P. A. (2011). "The terrestrial segment of soil moisture-climate coupling: SOIL MOISTURE-CLIMATE  
883 COUPLING." Geophysical Research Letters **38**(16): n/a-n/a.
- 884 Dorigo, W. A., W. Wagner, R. Hohensinn, S. Hahn, C. Paulik, A. Xaver, A. Gruber, M. Drusch, S. Mecklenburg, P.  
885 van Oevelen, A. Robock and T. Jackson (2011). "The International Soil Moisture Network: a data hosting facility  
886 for global in situ soil moisture measurements." Hydrology and Earth System Sciences **15**(5): 1675-1698.
- 887 Entekhabi, D., E. G. Njoku, P. E. O’Neill, K. H. Kellogg, W. T. Crow, W. N. Edelstein, J. K. Entin, S. D. Goodman,  
888 T. J. Jackson, J. Johnson, J. Kimball, J. R. Piepmeier, R. D. Koster, N. Martin, K. C. McDonald, M. Moghaddam, S.  
889 Moran, R. Reichle, J. C. Shi and J. Van Zyl (2010). "The Soil Moisture Active Passive (SMAP) Mission."  
890 Proceedings of the IEEE **98**(5): 704-716.
- 891 Farmani, M. A., A. A. Tavakoly, A. Behrangi, Y. Qiu, A. Gupta, M. Jawad, H. Y. Sohi, X.-Y. Zhang, M. P. Geheran  
892 and G. Niu (2024). "Improving Streamflow Predictions in the Arid Southwestern United States Through  
893 Understanding of Baseflow Generation Mechanisms."
- 894 Findell, K. L., P. Gentine, B. R. Lintner and C. Kerr (2011). "Probability of afternoon precipitation in eastern United  
895 States and Mexico enhanced by high evaporation." Nature Geoscience **4**(7): 434-439.
- 896 Gerke, H. H. and M. T. van Genuchten (1993). "A dual-porosity model for simulating the preferential movement of  
897 water and solutes in structured porous media." Water Resources Research **29**(2): 305-319.
- 898 Gerke, H. H. and M. T. van Genuchten (1993). "Evaluation of a first-order water transfer term for variably saturated  
899 dual-porosity flow models." Water Resources Research **29**(4): 1225-1238.
- 900 Gerke, H. H. and M. T. van Genuchten (1996). "Macroscopic representation of structural geometry for simulating  
901 water and solute movement in dual-porosity media." Advances in Water Resources **19**(6): 343-357.
- 902 Ghannam, K., T. Nakai, A. Paschalis, C. A. Oishi, A. Kotani, Y. Igarashi, T. Kumagai and G. G. Katul (2016).  
903 "Persistence and memory timescales in root-zone soil moisture dynamics." Water Resources Research **52**(2): 1427-  
904 1445.
- 905 Guo, Z., P. A. Dirmeyer, Z. Z. Hu, X. Gao and M. Zhao (2006). "Evaluation of the Second Global Soil Wetness  
906 Project soil moisture simulations: 2. Sensitivity to external meteorological forcing." Journal of Geophysical  
907 Research: Atmospheres **111**(D22).
- 908 Guo, Z., P. A. Dirmeyer, Z. Z. Hu, X. Gao and M. Zhao (2006). "Evaluation of the Second Global Soil Wetness  
909 Project soil moisture simulations: 2. Sensitivity to external meteorological forcing." Journal of Geophysical  
910 Research: Atmospheres **111**(D22): 2006JD007845.
- 911 He, Q., H. Lu and K. Yang (2023). "Soil Moisture Memory of Land Surface Models Utilized in Major Reanalyses  
912 Differ Significantly From SMAP Observation." Earth’s Future **11**(4).
- 913 Huffman, G. J., D. T. Bolvin, D. Braithwaite, K.-L. Hsu, R. J. Joyce, C. Kidd, E. J. Nelkin, S. Sorooshian, E. F.  
914 Stocker, J. Tan, D. B. Wolff and P. Xie (2020). Integrated Multi-satellite Retrievals for the Global Precipitation  
915 Measurement (GPM) Mission (IMERG). Satellite Precipitation Measurement: Volume 1. V. Levizzani, C. Kidd, D.  
916 B. Kirschbaum et al. Cham, Springer International Publishing: 343-353.

917 Jawad, M., B. Bhattacharya, A. Young and S. J. van Andel (2024). "Evaluation of Near Real-Time Global  
918 Precipitation Measurement (GPM) Precipitation Products for Hydrological Modelling and Flood Inundation  
919 Mapping of Sparsely Gauged Large Transboundary Basins—A Case Study of the Brahmaputra Basin." Remote  
920 Sensing **16**(10).

921 Katul, G. G., A. Porporato, E. Daly, A. C. Oishi, H. S. Kim, P. C. Stoy, J. Y. Juang and M. B. Siqueira (2007). "On  
922 the spectrum of soil moisture from hourly to interannual scales." Water Resources Research **43**(5): 2006WR005356.

923 Koster, R. D., P. A. Dirmeyer, Z. Guo, G. Bonan, E. Chan, P. Cox, C. T. Gordon, S. Kanae, E. Kowalczyk, D.  
924 Lawrence, P. Liu, C.-H. Lu, S. Malyshev, B. McAvaney, K. Mitchell, D. Mocko, T. Oki, K. Oleson, A. Pitman, Y.  
925 C. Sud, C. M. Taylor, D. Verseghy, R. Vasic, Y. Xue and T. Yamada (2004). "Regions of Strong Coupling Between  
926 Soil Moisture and Precipitation." Science **305**(5687): 1138-1140.

927 Koster, R. D., P. A. Dirmeyer, A. N. Hahmann, R. Ijpelaar, L. Tyahla, P. Cox and M. J. Suarez (2002). "Comparing  
928 the Degree of Land–Atmosphere Interaction in Four Atmospheric General Circulation Models." Journal of  
929 Hydrometeorology **3**(3): 363-375.

930 Koster, R. D., Z. Guo, R. Yang, P. A. Dirmeyer, K. Mitchell and M. J. Puma (2009). "On the Nature of Soil  
931 Moisture in Land Surface Models." Journal of Climate **22**(16): 4322-4335.

932 Koster, R. D., S. P. P. Mahanama, B. Livneh, D. P. Lettenmaier and R. H. Reichle (2010). "Skill in streamflow  
933 forecasts derived from large-scale estimates of soil moisture and snow." Nature Geoscience **3**(9): 613-616.

934 Koster, R. D. and S. P. P. Mahanama (2012). "Land Surface Controls on Hydroclimatic Means and Variability."  
935 Journal of Hydrometeorology **13**(5): 1604-1620.

936 Koster, R. D., R. H. Reichle and S. P. P. Mahanama (2017). "A Data-Driven Approach for Daily Real-Time  
937 Estimates and Forecasts of Near-Surface Soil Moisture." Journal of Hydrometeorology **18**(3): 837-843.

938 Koster, R. D., S. D. Schubert and M. J. Suarez (2009). "Analyzing the Concurrence of Meteorological Droughts and  
939 Warm Periods, with Implications for the Determination of Evaporative Regime." Journal of Climate **22**(12): 3331-  
940 3341.

941 Koster, R. D. and M. J. Suarez (1999). "A Simple Framework for Examining the Interannual Variability of Land  
942 Surface Moisture Fluxes." Journal of Climate **12**(7): 1911-1917.

943 Koster, R. D. and M. J. Suarez (2001). "Soil Moisture Memory in Climate Models." Journal of Hydrometeorology  
944 **2**(6): 558-570.

945 Mao, Y., W. T. Crow and B. Nijssen (2020). "A Unified Data-Driven Method to Derive Hydrologic Dynamics From  
946 Global SMAP Surface Soil Moisture and GPM Precipitation Data." Water Resources Research **56**(2):  
947 e2019WR024949.

948 McColl, K. A., S. H. Alemohammad, R. Akbar, A. G. Konings, S. Yueh and D. Entekhabi (2017). "The global  
949 distribution and dynamics of surface soil moisture." Nature Geoscience **10**(2): 100-104.

950 McColl, K. A., Q. He, H. Lu and D. Entekhabi (2019). "Short-Term and Long-Term Surface Soil Moisture Memory  
951 Time Scales Are Spatially Anticorrelated at Global Scales." Journal of Hydrometeorology **20**(6): 1165-1182.

952 McColl, K. A., W. Wang, B. Peng, R. Akbar, D. J. Short Gianotti, H. Lu, M. Pan and D. Entekhabi (2017). "Global  
953 characterization of surface soil moisture drydowns." Geophysical Research Letters **44**(8): 3682-3690.

954 Mei, R. and G. Wang (2012). "Summer Land–Atmosphere Coupling Strength in the United States: Comparison  
955 among Observations, Reanalysis Data, and Numerical Models." Journal of Hydrometeorology **13**(3): 1010-1022.

956 Moghisi, S. S., J. Yazdi and S. A. A. Salehi Neyshabouri (2024). "Multivariate Analysis of Rainfall Spatial  
957 Distribution and Its Effect on Stormwater Magnitudes." Journal of Hydrologic Engineering **29**(2): 05024002.

958 Mohammadi, Y., O. Zandi, M. Nasser and Y. Rashidi (2023). "Spatiotemporal modeling of PM10 via committee  
959 method with in-situ and large scale information: Coupling of machine learning and statistical methods." Urban  
960 Climate **49**.

961 Nakai, T., G. G. Katul, A. Kotani, Y. Igarashi, T. Ohta, M. Suzuki and T. o. Kumagai (2014). "Radiative and  
962 precipitation controls on root zone soil moisture spectra." Geophysical Research Letters **41**(21): 7546-7554.

963 Niu, G., Y. Fang, A. A. M. Neto, B. Guo, X.-Y. Zhang, M. A. Farmani, A. Behrangi and X. Zeng (2024).  
964 "Representing Preferential Flow through Variably-Saturated Soils with Surface Ponding in a Large-Scale Land  
965 Surface Model over the Conterminous US."

966 Niu, G.-Y., Z.-L. Yang, K. E. Mitchell, F. Chen, M. B. Ek, M. Barlage, A. Kumar, K. Manning, D. Niyogi, E.  
967 Rosero, M. Tewari and Y. Xia (2011). "The community Noah land surface model with multiparameterization  
968 options (Noah-MP): 1. Model description and evaluation with local-scale measurements." Journal of Geophysical  
969 Research **116**(D12): D12109.

970 Niu, G. Y., Y. H. Fang, L. L. Chang, J. Jin, H. Yuan and X. Zeng (2020). "Enhancing the Noah-MP Ecosystem  
971 Response to Droughts With an Explicit Representation of Plant Water Storage Supplied by Dynamic Root Water  
972 Uptake." Journal of Advances in Modeling Earth Systems **12**(11).

973 Oleson, K., D. Lawrence, G. Bonan, M. Flanner, E. Kluzek, P. Lawrence, S. Levis, S. Swenson, P. Thornton, A.  
974 Dai, M. Decker, R. Dickinson, J. Feddema, C. Heald, F. Hoffman, J.-F. Lamarque, N. Mahowald, G.-Y. Niu, T.  
975 Qian, J. Randerson, S. Running, K. Sakaguchi, A. Slater, R. Stockli, A. Wang, Z.-L. Yang, X. Zeng and X. Zeng  
976 (2010). Technical Description of version 4.0 of the Community Land Model (CLM), UCAR/NCAR: 2612 KB.  
977 Pastorello, G., C. Trotta, E. Canfora, H. Chu, D. Christianson, Y.-W. Cheah, C. Poindexter, J. Chen, A. Elbashandy,  
978 M. Humphrey, P. Isaac, D. Polidori, M. Reichstein, A. Ribeca, C. Van Ingen, N. Vuichard, L. Zhang, B. Amiro, C.  
979 Ammann, M. A. Arain, J. Ardö, T. Arkebauer, S. K. Arndt, N. Arriga, M. Aubinet, M. Aurela, D. Baldocchi, A.  
980 Barr, E. Beamesderfer, L. B. Marchesini, O. Bergeron, J. Beringer, C. Bernhofer, D. Berveiller, D. Billesbach, T. A.  
981 Black, P. D. Blanken, G. Bohrer, J. Boike, P. V. Bolstad, D. Bonal, J.-M. Bonnefond, D. R. Bowling, R. Bracho, J.  
982 Brodeur, C. Brümmer, N. Buchmann, B. Burban, S. P. Burns, P. Buysse, P. Cale, M. Cavagna, P. Cellier, S. Chen, I.  
983 Chini, T. R. Christensen, J. Cleverly, A. Collalti, C. Consalvo, B. D. Cook, D. Cook, C. Coursolle, E. Cremonese, P.  
984 S. Curtis, E. D'Andrea, H. Da Rocha, X. Dai, K. J. Davis, B. D. Cinti, A. D. Grandcourt, A. D. Ligne, R. C. De  
985 Oliveira, N. Delpierre, A. R. Desai, C. M. Di Bella, P. D. Tommasi, H. Dolman, F. Domingo, G. Dong, S. Dore, P.  
986 Duce, E. Dufrière, A. Dunn, J. Dušek, D. Eamus, U. Eichelmann, H. A. M. ElKhidir, W. Eugster, C. M. Ewenz, B.  
987 Ewers, D. Famulari, S. Fares, I. Feigenwinter, A. Feitz, R. Fensholt, G. Filippa, M. Fischer, J. Frank, M. Galvagno,  
988 M. Gharun, D. Gianelle, B. Gielen, B. Gioli, A. Gitelson, I. Goded, M. Goeckede, A. H. Goldstein, C. M. Gough, M.  
989 L. Goulden, A. Graf, A. Griebel, C. Gruening, T. Grünwald, A. Hammerle, S. Han, X. Han, B. U. Hansen, C.  
990 Hanson, J. Hatakka, Y. He, M. Hehn, B. Heinesch, N. Hinko-Najera, L. Hörtnagl, L. Hutley, A. Ibrom, H. Ikawa, M.  
991 Jackowicz-Korczynski, D. Janouš, W. Jans, R. Jassal, S. Jiang, T. Kato, M. Khomik, J. Klatt, A. Knohl, S. Knox, H.  
992 Kobayashi, G. Koerber, O. Kolle, Y. Kosugi, A. Kotani, A. Kowalski, B. Kruijt, J. Kurbatova, W. L. Kutsch, H.  
993 Kwon, S. Launiainen, T. Laurila, B. Law, R. Leuning, Y. Li, M. Liddell, J.-M. Limousin, M. Lion, A. J. Liska, A.  
994 Lohila, A. López-Ballesteros, E. López-Blanco, B. Loubet, D. Loustau, A. Lucas-Moffat, J. Lüers, S. Ma, C.  
995 Macfarlane, V. Magliulo, R. Maier, I. Mammarella, G. Manca, B. Marcolla, H. A. Margolis, S. Marras, W.  
996 Massman, M. Mastepanov, R. Matamala, J. H. Matthes, F. Mazzenga, H. McCaughey, I. McHugh, A. M. S.  
997 McMillan, L. Merbold, W. Meyer, T. Meyers, S. D. Miller, S. Minerbi, U. Moderow, R. K. Monson, L. Montagnani,  
998 C. E. Moore, E. Moors, V. Moreaux, C. Moureaux, J. W. Munger, T. Nakai, J. Neiryneck, Z. Nesic, G. Nicolini, A.  
999 Noormets, M. Northwood, M. Noretto, Y. Nouvellon, K. Novick, W. Oechel, J. E. Olesen, J.-M. Ourcival, S. A.  
1000 Papuga, F.-J. Parmentier, E. Paul-Limoges, M. Pavelka, M. Peichl, E. Pendall, R. P. Phillips, K. Pilegaard, N. Pirk,  
1001 G. Posse, T. Powell, H. Prasse, S. M. Prober, S. Rambal, Ü. Rannik, N. Raz-Yaseef, C. Rebmann, D. Reed, V. R. D.  
1002 Dios, N. Restrepo-Coupe, B. R. Reverter, M. Roland, S. Sabbatini, T. Sachs, S. R. Saleska, E. P. Sánchez-Cañete, Z.  
1003 M. Sanchez-Mejia, H. P. Schmid, M. Schmidt, K. Schneider, F. Schrader, I. Schroder, R. L. Scott, P. Sedláč, P.  
1004 Serrano-Ortiz, C. Shao, P. Shi, I. Shironya, L. Siebicke, L. Šigut, R. Silberstein, C. Sirca, D. Spano, R. Steinbrecher,  
1005 R. M. Stevens, C. Sturtevant, A. Suyker, T. Tagesson, S. Takanashi, Y. Tang, N. Tapper, J. Thom, M. Tomassucci,  
1006 J.-P. Tuovinen, S. Urbanski, R. Valentini, M. Van Der Molen, E. Van Gorsel, K. Van Huissteden, A. Varlagin, J.  
1007 Verfaillie, T. Vesala, C. Vincke, D. Vitale, N. Vygodskaya, J. P. Walker, E. Walter-Shea, H. Wang, R. Weber, S.  
1008 Westermann, C. Wille, S. Wofsy, G. Wohlfahrt, S. Wolf, W. Woodgate, Y. Li, R. Zampedri, J. Zhang, G. Zhou, D.  
1009 Zona, D. Agarwal, S. Biraud, M. Torn and D. Papale (2020). "The FLUXNET2015 dataset and the ONEFlux  
1010 processing pipeline for eddy covariance data." *Scientific Data* 7(1): 225.  
1011 Poggio, L., L. M. de Sousa, N. H. Batjes, G. B. M. Heuvelink, B. Kempen, E. Ribeiro and D. Rossiter (2021).  
1012 "SoilGrids 2.0: producing soil information for the globe with quantified spatial uncertainty." *Soil* 7(1): 217-240.  
1013 Seneviratne, S. I. and R. D. Koster (2012). "A Revised Framework for Analyzing Soil Moisture Memory in Climate  
1014 Data: Derivation and Interpretation." *Journal of Hydrometeorology* 13(1): 404-412.  
1015 Seneviratne, S. I., R. D. Koster, Z. Guo, P. A. Dirmeyer, E. Kowalczyk, D. Lawrence, P. Liu, D. Mocko, C.-H. Lu,  
1016 K. W. Oleson and D. Verseghy (2006). "Soil Moisture Memory in AGCM Simulations: Analysis of Global Land-  
1017 Atmosphere Coupling Experiment (GLACE) Data." *Journal of Hydrometeorology* 7(5): 1090-1112.  
1018 Seneviratne, S. I., D. Lüthi, M. Litschi and C. Schär (2006). "Land-atmosphere coupling and climate change in  
1019 Europe." *Nature* 443(7108): 205-209.  
1020 Shellito, P. J., E. E. Small, A. Colliander, R. Bindlish, M. H. Cosh, A. A. Berg, D. D. Bosch, T. G. Caldwell, D. C.  
1021 Goodrich, H. McNairn, J. H. Prueger, P. J. Starks, R. Van Der Velde and J. P. Walker (2016). "SMAP soil moisture  
1022 drying more rapid than observed in situ following rainfall events." *Geophysical Research Letters* 43(15): 8068-8075.  
1023 Shellito, P. J., E. E. Small and B. Livneh (2018). "Controls on surface soil drying rates observed by SMAP and  
1024 simulated by the Noah land surface model." *Hydrology and Earth System Sciences* 22(3): 1649-1663.  
1025 Šimůnek, J. and M. T. Van Genuchten (2008). "Modeling Nonequilibrium Flow and Transport Processes Using  
1026 HYDRUS." *Vadose Zone Journal* 7(2): 782-797.  
1027 Souri, J., H. OmidvarMohammadi, S. A. A. S. Neyshabouri, C. A. Chooplou, E. Kahrizi, H. Akbari, J. Souri, H.  
1028 OmidvarMohammadi, S. A. A. S. Neyshabouri, C. A. Chooplou, E. Kahrizi and H. Akbari (2024). "Numerical

1029 simulation of aeration impact on the performance of a-type rectangular and trapezoidal piano key weirs." Modeling  
1030 Earth Systems and Environment 2024 10:4 10(4).

1031 Taylor, C. M., C. E. Birch, D. J. Parker, N. Dixon, F. Guichard, G. Nikulin and G. M. S. Lister (2013). "Modeling  
1032 soil moisture-precipitation feedback in the Sahel: Importance of spatial scale versus convective parameterization."  
1033 Geophysical Research Letters 40(23): 6213-6218.

1034 Tuttle, S. and G. Salvucci (2016). "Empirical evidence of contrasting soil moisture-precipitation feedbacks across  
1035 the United States." Science 352(6287): 825-828.

1036 Xia, Y., K. Mitchell, M. Ek, J. Sheffield, B. Cosgrove, E. Wood, L. Luo, C. Alonge, H. Wei, J. Meng, B. Livneh, D.  
1037 Lettenmaier, V. Koren, Q. Duan, K. Mo, Y. Fan and D. Mocko (2012). "Continental-scale water and energy flux  
1038 analysis and validation for the North American Land Data Assimilation System project phase 2 (NLDAS-2): 1.  
1039 Intercomparison and application of model products." Journal of Geophysical Research: Atmospheres 117(D3).

1040 Yang, K., Y. Chen, J. He, L. Zhao, H. Lu, J. Qin, D. Zheng and X. Li (2020). "Development of a daily soil moisture  
1041 product for the period of 2002–2011 in Chinese mainland." Science China Earth Sciences 63(8): 1113-1125.

1042 Yang, Z.-L., G.-Y. Niu, K. E. Mitchell, F. Chen, M. B. Ek, M. Barlage, L. Longuevergne, K. Manning, D. Niyogi,  
1043 M. Tewari and Y. Xia (2011). "The community Noah land surface model with multiparameterization options (Noah-  
1044 MP): 2. Evaluation over global river basins." Journal of Geophysical Research 116(D12): D12110.

1045 Yousefi Sohi, H., M. A. Farmani and A. Behrangi (2024). "How do IMERG V07, IMERG V06, and ERA5  
1046 Precipitation Products Perform Over Snow-ice-free and Snow-ice-covered Surfaces at a Range of Near Surface  
1047 Temperatures?" ESS Open Archive.

1048 Yousefi Sohi, H., B. Zahraie, N. Dolatabadi and F. Zebarjadian (2024). "Application of VIC-WUR model for  
1049 assessing the spatiotemporal distribution of water availability in anthropogenically-impacted basins." Journal of  
1050 Hydrology 637.

1051 Zebarjadian, F., N. Dolatabadi, B. Zahraie, H. Yousefi Sohi and O. Zandi (2024). "Triple coupling random forest  
1052 approach for bias correction of ensemble precipitation data derived from Earth system models for Divandareh-Bijar  
1053 Basin (Western Iran)." International Journal of Climatology 44(7): 2363-2390.

1054 Zeng, X., J. Liu, Z. Ma, S. Song, C. Xi and H. Wang (2010). "Study on the effects of land surface heterogeneities in  
1055 temperature and moisture on annual scale regional climate simulation." Advances in Atmospheric Sciences 27(1):  
1056 151-163.

1057 Zhang, X., G.-Y. Niu, A. S. Elshall, M. Ye, G. A. Barron-Gafford and M. Pavao-Zuckerman (2014). "Assessing five  
1058 evolving microbial enzyme models against field measurements from a semiarid savannah-What are the mechanisms  
1059 of soil respiration pulses?" Geophysical Research Letters 41(18): 6428-6434.

1060  
1061  
1062